Unitary coupled-channels model for three-mesons decays of heavy mesons

H. Kamano, S. X. Nakamura, T.-S. H. Lee, and T. Sato

Phys. Rev. D **84**, 114019 — Published 16 December 2011

DOI: 10.1103/PhysRevD.84.114019

Unitary coupled-channels model for three-mesons decays of heavy mesons

H. Kamano,[1,2] S. X. Nakamura,[2] T.-S. H. Lee,[3,2] and T. Sato[4,2]

[1]*Research Center for Nuclear Physics, Osaka University, Ibaraki, Osaka 567-0047, Japan*

[2]*Excited Baryon Analysis Center (EBAC), Thomas Jefferson National Accelerator Facility, Newport News, Virginia 23606, USA*

[3]*Physics Division, Argonne National Laboratory, Argonne, Illinois 60439, USA*

[4]*Department of Physics, Osaka University, Toyonaka, Osaka 560-0043, Japan*

Abstract

A unitary coupled-channels model is presented for investigating the decays of heavy mesons and excited meson states into three light pseudoscalar mesons. The model accounts for the three-mesons final state interactions in the decay processes, as required by both the three-body and two-body unitarity conditions. In the absence of the Z-diagram mechanisms that are necessary consequence of the three-body unitarity, our decay amplitudes are reduced to a form similar to those used in the so-called isobar-model analysis. We apply our coupled-channels model to the three-pions decays of $a_1(1260)$, $\pi_2(1670)$, $\pi_2(2100)$, and D^0 mesons, and show that the Z-diagram mechanisms can contribute to the calculated Dalitz plot distributions by as much as 30% in magnitudes in the regions where $f_0(600)$, $\rho(770)$, and $f_2(1270)$ dominate the distributions. Also, by fitting to the same Dalitz plot distributions, we demonstrate that the decay amplitudes obtained with the unitary model and the isobar model can be rather different, particularly in the phase that plays a crucial role in extracting the CKM CP-violating phase from the data of B meson decays. Our results indicate that the commonly used isobar model analysis must be extended to account for the final state interactions required by the three-body unitarity to re-analyze the three-mesons decays of heavy mesons, thereby exploring hybrid or exotic mesons, and signatures of physics beyond the Standard Model.

PACS numbers: 13.25.-k,14.40.Rt,11.80.Jy

Keywords: heavy-meson hadronic decay, exotic meson, 3-body unitarity

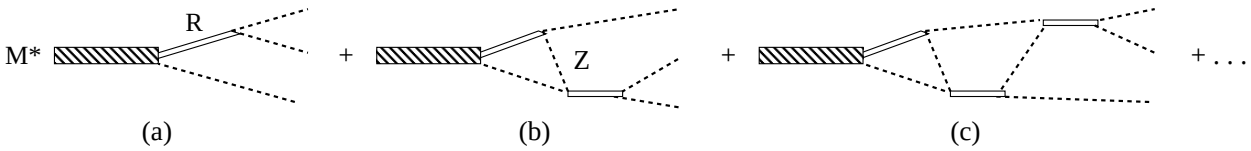

FIG. 1. M^*-decay amplitude.

I. INTRODUCTION

It has long been recognized that hadrons lying outside of the conventional constituent quark model must exist within the framework of Quantum Chromodynamics (QCD). These so-called "exotic" hadrons, speculated as tetra-quark states or hybrid states or glueballs, have been predicted by various calculations using the Lattice QCD, the QCD sum rule, and the flux-tube model, as reviewed in Ref. [1]. Thus, quite a few experimental programs have been developed to search for exotic mesons via the three-mesons production reactions, such as $\pi N \to M^* N \to \pi\pi\pi N$ [2–4], $\gamma N \to M^* N \to \pi\pi\pi N, \pi K\bar{K}N$ [5, 6], and $N\bar{N} \to M^* \to \pi\pi\eta$ [7], where the intermediate mesons M^* could be exotic. To identify M^*, the main task is to extract the partial-wave amplitudes from the final three-mesons distributions. So far, this has been done mainly by using the isobar model, within which two of the three mesons form a light flavor excited meson R (f_0, ρ, K^*, etc.) and the third meson is treated as a spectator in the decays of R, as illustrated in Fig. 1(a). There, the propagation of R is commonly described with the Breit-Wigner parametrization or with the two-body unitary K-matrix parameterizations [8, 9] constrained by the dispersion relations. In any case, the three-body unitarity is missing in those analyses. The non-interacting cR amplitudes, where c is a spectator light pseudoscalar meson, and an appropriately parametrized non-resonant amplitude are then summed coherently with multiplicative complex parameters which are adjusted to fit the Dalitz plot of the measured three-mesons distributions.

In an isobar model analysis of the $\pi^- p \to \pi^-\pi^-\pi^+ p$ and $\pi^- p \to \pi^-\pi^0\pi^0 p$ data from the E852 experiment [2–4], $a_1(1260)$, $a_2(1320)$, $\pi_2(1670)$ and $a_4(2020)$ resonances were identified, and the exotic $J^{PC} = 1^{-+}$ meson near 1.6 GeV [$\pi_1(1600)$] proposed from an earlier analysis was ruled out. The CLAS analysis [6] of $\gamma p \to \pi^+\pi^+\pi^- n$ data identified $a_2(1320)$ and $\pi_2(1670)$, but not $a_1(1260)$, and nor exotic $\pi_1(1600)$ at the expected levels. On the other hand, the COMPASS experiment [10] claimed to have observed $\pi_1(1600)$ in the $\pi^-\pi^-\pi^+$ final state from a pion scattering on a lead target. As a step to understand the differences

between the results from these analyses as well as from the previous isobar model analyses, it is necessary to first examine the extent to which the isobar model is valid. This is also needed for developing a theoretically sound approach to analyze the three-mesons photoproduction data that will be obtained at JLab with the 12-GeV upgrade [5].

The isobar model has also been commonly used to analyze the data of three-mesons decays of J/ψ [11, 12], D [13–23] and B [24–35] mesons. The B and D decays have been analyzed with interests in the CP violation and physics beyond the Standard Model. Some B decay processes have also been analyzed using dispersion relations [36], neglecting the interactions between the outgoing two-mesons subsystem and the third meson, as assumed in the isobar model. The strong phases arising from the final state interactions in the decay processes are essential in determining the weak decay amplitudes of these heavy mesons and searching for physics beyond the Standard Model. For example, BABAR [18, 20, 21] and Belle [22, 23] extracted the Cabibbo-Kobayashi-Maskawa (CKM) CP violating phase γ from the data of $B^{\mp} \to D^0$ (or $\bar{D}^0$) $K^{\mp} \to (K^0_S\pi^+\pi^-)K^{\mp}$. They utilized the fact that the interference between the decay amplitude of $B^{\mp} \to D^0K^{\mp} \to (K^0_S\pi^+\pi^-)K^{\mp}$ and that of $B^{\mp} \to \bar{D}^0K^{-} \to (K^0_S\pi^+\pi^-)K^{\mp}$ is proportional to $e^{\mp i\gamma}$. Clearly, the accuracy of the phases of the partial-wave amplitudes of $D^0(\bar{D}^0) \to (K^0_S\pi^+\pi^-)$, which were determined within the isobar model, is crucial in extracting this fundamental parameters γ from the data. In the isobar model, the strong phases from the final state interactions are partly accounted for by using complex $D \to \pi R$ couplings. However, the phases of the amplitudes generally depend on kinematics and has to satisfy the three-body unitarity, which is beyond what the isobar model can achieve.

The above discussions strongly indicate the need of investigating the extent to which the isobar model is valid. Within the well-developed three-hadron scattering models, as reviewed in Refs. [37–39], the isobar model is clearly a simplification since one of the meson from the decay of the propagating resonance R can interact with the third meson to form another R. This interaction is traditionally called the Z-diagram, as illustrated in Fig. 1(b). It was well established in the studies of πN [37], πNN [38] and $\pi\pi N$ [39–41] systems that the multiple scattering due to the Z-diagram mechanisms, as illustrated in Fig. 1(c), is essential to preserve the three-body unitarity for interpreting the data correctly. Only very limited similar attempts have been taken recently to analyze the three-mesons decay of heavy mesons [42, 43].

The main purpose of this work is to apply the unitary approach developed in Ref. [39] (Hereafter we refer it as MSL.) to investigate the importance of the Z-diagram mechanisms in analyzing the data of three-mesons decays from heavy mesons and excited meson states. We will present a model that satisfies the two-body and three-body unitarity conditions. We start with a model Hamiltonian defined by (bare) vertex interactions $f_{ab,R}$ and Γ_{cR,M^*} and two-body interactions $v_{c'R',cR}$, where a, b, c are physical light pseudoscalar mesons (π, K etc.), R is a light flavor excited state decaying to two light pseudoscalar mesons, $R = f_0, \rho, f_2, K^*, ...$, and M^* is a heavy meson decaying to three light pseudoscalar mesons. The vertex interactions $f_{ab,R}$ are determined by fitting the empirical $ab \to ab$ scattering amplitudes, and are used to define the propagation of R and to calculate the one-particle-exchange Z-diagram amplitudes $Z_{c'R',cR}$. The $cR \to c'R'$ scattering amplitudes $T_{c'R',cR}$ are then calculated from $Z_{c'R',cR}$ by solving a set of coupled-channels equations to account for the three-mesons final state interactions of heavy-meson decays. In the absence of the Z-diagram mechanisms, our decay amplitudes are reduced to a form similar to those used in the isobar-model analysis. Thus we will be able to examine the effects of Z-diagram mechanisms in determining the Dalitz plots and the parameters of resonances which decay strongly into three-mesons. The model is applied to investigate the three-pions decays of $a_1(1260)$, $\pi_2(1670)$, $\pi_2(2100)$, and D^0 mesons.

The organization of this paper is as follows. In Sec. II, we present our model Hamiltonian and describe the derivation of a set of coupled-channel equations for calculating the meson-R scattering amplitudes from the Z-diagram mechanisms, and how these amplitudes are used to calculate the three-mesons final state interactions in heavy meson decays. The procedures for applying our model in practical calculations are given in Sec. III. The results for calculations of the decays of $a_1(1260)$, $\pi_2(1670)$, $\pi_2(2100)$, and D^0 mesons are presented in Sec. IV. Summary and outlook are given in Sec. V.

II. FORMULATION

Following the MSL formulation [39] of hadron reactions, we assume that the decays of heavy mesons into three mesons can be described by the following Hamiltonian,

$$H = H_0 + H', \tag{1}$$

where H_0 is the free Hamiltonian of the considered degrees of freedom: the bare heavy mesons $M^* = a_1, \pi_2, D^0, ...$, the bare light flavor excited mesons $R = f_0, \rho, f_2, ...$, and the physical ground pseudoscalar mesons denoted as $a, b, c = \pi$, K etc. The interaction Hamiltonian H' is defined as (In this section, the summation runs over the momentum, spin, and isospin spaces of the particles.),

$$H' = \sum_{cR} [\Gamma_{cR,M^*} + \Gamma^\dagger_{cR,M^*}] + H'', \tag{2}$$

$$H'' = \sum_{c'R',cR} v_{c'R',cR} + \sum_R \sum_{ab} [f_{ab,R} + f^\dagger_{ab,R}], \tag{3}$$

where $v_{c'R',cR}$ denotes the $cR \to c'R'$ transition potentials; Γ_{cR,M^*} ($f_{ab,R}$) is the bare vertex describing $M^* \to cR$ ($R \to ab$) processes. Here we note that the term H'' does not include any interactions with the M^* states and we have neglected the interactions between the particles (a,b) in the decay channels of the light flavor excited meson states R. Throughout this paper, we will use the "right-to-left" ordering for the channel indices. (Note that $\Gamma_{M^*,cR} = \Gamma^\dagger_{cR,M^*}$ and $f_{R,ab} = f^\dagger_{ab,R}$ for the bare vertices.)

Starting with Eq. (1), the reaction T-matrix is defined by the following equation,

$$T(E) = H' + H' \frac{1}{E - H + i\epsilon} H', \tag{4}$$

where E is the total scattering energy in the center of mass system. Since the considered Hamiltonian is hermitian and energy independent, it is straightforward to show that the S-matrix $S(E) = 1 - 2\pi i \delta(E - H_0) T(E)$ is unitary $S^\dagger(E) S(E) = 1$. This is the simplicity of this formulation to have a unitary reaction model. To solve Eq. (4), it is convenient to first define a scattering equation for calculating the effects only from the non-M^* Hamiltonian H'' on the scattering of the ground pseudoscalar mesons $c = \pi, K$ from the light flavor excited meson states $R = f_0, \rho, f_2, ...$ Namely, we will first calculate the amplitude

$$T'_{c'R',cR}(E) = \langle c'R' | T'(E) | cR \rangle$$

where the non-M^* scattering operator $T'(E)$ is defined by

$$T'(E) = H'' + H'' \frac{P}{E - H_0 - H'' + i\epsilon} H''. \tag{5}$$

The intermediate states in the above equation are restricted by the projection operator P defined by

$$P = \sum_{cR} |cR\rangle\langle cR| + \sum_{abc} |abc\rangle\langle abc|. \tag{6}$$

By further applying the standard projection operator method [44, 45], as detailed in Ref. [39] for a $\pi\pi N$ Hamiltonian, one can cast Eq. (5) into a form for practical calculations of $T'_{c'R',cR}(E)$. By simply changing the particle labels and dropping the contributions from the direct γ_{13}, v_{23}, v_{33} interactions in the Appendix B of Ref. [39], we can obtain the scattering amplitudes for this investigation. The resulting $cR \to c'R'$ amplitudes, which describe the multiple scattering mechanisms followed by a M^* decay as illustrated in Figs. 1(b) and 1(c), are defined by

$$T'_{c'R',cR}(E) = V_{c'R',cR}(E) + \sum_{c'''R''',c''R''} V_{c'R',c'''R'''}(E) G_{c'''R''',c''R''}(E) T'_{c''R'',cR}(E). \tag{7}$$

Here the driving term is

$$V_{c'R',cR}(E) = v_{c'R',cR} + Z_{c'R',cR}(E), \tag{8}$$

where $v_{c'R',cR}$ is the $cR \to c'R'$ transition potential, and the second term is the Z-diagram defined with the $R \to ab$ vertex as

$$Z_{c'R',cR}(E) = \sum_{c''} f_{R',cc''} \frac{1}{E - E_c - E_{c'} - E_{c''} + i\epsilon} f_{c'c'',R}. \tag{9}$$

Here c'' is the exchanged meson. We have also introduced a notation $E_c = \sqrt{m_c^2 + \vec{p}_c^{\,2}}$ to denote the free energy operator for a particle c with mass m_c and momentum $\vec{p}_c$.

The Green function in Eq. (7) is defined by

$$[G^{-1}(E)]_{c'R',cR} = \delta_{c',c} \left[(E - E_c - E_R)\delta_{R',R} - \Sigma_{R',R}(E - E_c) \right]. \tag{10}$$

The self-energy of the propagation of R in Eq. (10) is

$$\Sigma_{R',R}(w) = \sum_{ab} \langle R' | f_{R',ab} \frac{\mathcal{B}_{ab}}{w - E_a - E_b + i\epsilon} f_{ab,R} | R \rangle, \tag{11}$$

where $\mathcal{B}_{ab}$ is a factor associated with the Bose symmetry of mesons: $\mathcal{B}_{ab} = 1/2$ if a and b are the identical particles or otherwise $\mathcal{B}_{ab} = 1$.

The self-energy (11) also determines the $ab \to a'b'$ scattering amplitudes. In the center of mass system, it has the familiar form

$$T_{a'b',ab}(w) = \sum_{R,R'} (\mathcal{B}_{a'b'})^{1/2} f_{a'b',R'} [d^{-1}(w)]_{R',R} (\mathcal{B}_{ab})^{1/2} f_{R,ab}, \tag{12}$$

with

$$[d(w)]_{R',R} = (w - m_R)\delta_{R',R} - \Sigma_{R',R}(w). \tag{13}$$

We thus can determine the mass m_R of bare R state and the vertex interaction $f_{ab,R}$ by fitting the empirical amplitudes of the meson-meson scatterings such as $\pi\pi \to \pi\pi$ and $\pi K \to \pi K$. This then allows us to predict the Z-diagram effects on $T'_{c'R',cR}$ through solving Eq. (7).

The transition potential $v_{c'R',cR}$ can be derived from phenomenological Lagrangian by using the method of unitary transformation [39, 46]. It can also be taken from more fundamental modelings within QCD. This is beyond the scope of this paper, and we set $v_{c'R',cR} = 0$ in solving Eq. (7). Thus the final three-mesons scattering effects predicted in this work is only the necessary consequence of meson-meson scattering under the three-body unitarity condition.

The amplitude for the three-mesons decay of M^*, $M^* \to abc$, is

$$T_{abc,M^*}(E) = \langle \Psi^{(-)}_{abc}(E)|H'|M^*\rangle, \tag{14}$$

where the three-mesons scattering wave function is defined by

$$\langle \Psi^{(-)}_{abc}(E)| = \langle abc| \left[1 + H'' \frac{1}{E - \bar{H} + i\epsilon}\right], \tag{15}$$

with $\langle abc|$ being the three-mesons plane-wave state. From Eqs. (2) and (3), we see that

$$H'|M^*\rangle = \sum_{cR} |cR\rangle\langle cR|\Gamma_{cR,M^*}|M^*\rangle,$$

$$\langle abc|H'' = \sum_{(a'b'c')}^{\text{cyclic}} \sum_{R} \langle abc|f_{a'b',R}|c'R\rangle\langle c'R|.$$

Here the symbol $\sum_{(a'b'c')}^{\text{cyclic}}$ means taking summation over the cyclic permutation, $(a'b'c') = (abc), (cab), (bca)$. Because of the orthogonality conditions, $\langle cR|M^*\rangle = 0$ and $\langle abc|cR\rangle = 0$, the above relations allow us to write Eq. (14) as

$$T_{abc,M^*}(E) = \langle abc|H'' \left[P_D \frac{1}{E - \bar{H} + i\epsilon} P_D\right] H'|M^*\rangle, \tag{16}$$

where P_D is the projection operator for the space spanned by cR states,

$$P_D = \sum_{cR} |cR\rangle\langle cR|. \tag{17}$$

Following the procedures in the Appendix B of Ref. [39], one can show that

$$\begin{aligned} P_D \frac{1}{E - \bar{H} + i\epsilon} P_D = & \sum_{c'R',cR} |c'R'\rangle G_{c'R',cR}(E)\langle cR| \\ & + \sum_{cR,c'R'} \sum_{c'''R''',c''R''} |c'R'\rangle G_{c'R',c'''R'''}(E) T'_{c'''R''',c''R''}(E) G_{c''R'',cR}(E)\langle cR|, \end{aligned} \tag{18}$$

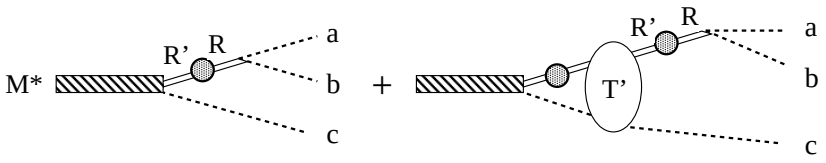

FIG. 2. Amplitude for the three-mesons decays of M^* in the unitary coupled-channels model. The bulb labeled T' is the T-matrix element for the $cR \to c'R'$ process without M^* excitation [Eq. (7)]. The dressing cR Green function, yielding $G_{cR,cR'}(E)$, is indicated by the gray circle [Eq. (10)].

where $T'_{c'''R''',c''R''}(E)$ and $G_{cR,c'R'}(E)$ have been defined in Eqs. (7) and (10), respectively.

Substituting Eq. (18) into Eq. (16) and using the vertex functions of H' defined by Eq. (2), we can write

$$T_{abc,M^*}(E) = \sum_{(a'b'c')}^{\text{cyclic}} T_{(a'b')c',M^*}(E), \tag{19}$$

with $T_{(ab)c,M^*}(E)$ being the amplitude for the subsequent decay of $M^* \to Rc \to (ab)c$ expressed as

$$T_{(ab)c,M^*}(E) = T^{\text{Isobar}}_{(ab)c,M^*}(E) + T^{\text{FSI}}_{(ab)c,M^*}(E), \tag{20}$$

where

$$T^{\text{Isobar}}_{(ab)c,M^*}(E) = \sum_R \sum_{c'R'} \langle ab| f_{ab,R} G_{cR,c'R'}(E) \Gamma_{c'R',M^*} |M^*\rangle, \tag{21}$$

$$T^{\text{FSI}}_{(ab)c,M^*}(E) = \sum_R \sum_{c'R'} \sum_{c'''R''',c''R''} \langle ab| f_{ab,R} G_{cR,c'R'}(E) T'_{c'R',c'''R'''}(E) G_{c'''R''',c''R''}(E) \Gamma_{c''R'',M^*} |M^*\rangle. \tag{22}$$

Equation (20) is illustrated in Fig. 2. We now note that the commonly used isobar model analysis corresponds to keeping only the term $T^{\text{Isobar}}_{abc,M^*}(E)$ within our formulation. The difference between different isobar analyses are in the parametrization of the Green function $G_{cR,c'R'}(E)$ and the vertex function $f_{ab,R}$. We also note that even in this simplified case, $G_{cR,c'R'}(E)$ and $f_{ab,R}$ are related through Eqs. (10) and (11) within our formulation, but are often not treated consistently in the isobar model analysis.

The full decay amplitude (20) can be concisely written as

$$T_{(ab)c,M^*}(E) = \sum_R \sum_{c'R'} \langle ab| f_{ab,R} G_{cR,c'R'}(E) |\bar{\Gamma}_{c'R',M^*}\rangle, \tag{23}$$

where the dressed $M^* \to cR$ vertex function is defined by

$$|\bar{\Gamma}_{cR,M^*}\rangle = \sum_{c''R''} \left[\delta_{cR,c''R''} + \sum_{c'''R'''} T'_{cR,c'''R'''} G_{c'''R''',c''R''}(E) \right] \Gamma_{c''R'',M^*} |M^*\rangle. \tag{24}$$

Obviously, $T^{\rm Isobar}_{(ab)c,M^*}(E)$ of Eq. (21) can be obtained from Eq. (23) by replacing $|\bar{\Gamma}_{c'R',M^*}\rangle$ with $\Gamma_{c'R',M^*}|M^*\rangle$.

For strong decays, the resonance pole positions and decay widths of heavy mesons (M^*) can be shifted by three-mesons scattering. This can be seen by considering the M^* propagator defined by

$$G_{M^*}(E) = \langle M^*| \frac{1}{E - H + i\epsilon} |M^*\rangle. \tag{25}$$

With the projection operator method, as applied in Ref. [39], one can show that Eq. (25) in the rest frame of M^* can be written as

$$G^{-1}_{M^*}(E) = E - M^0_{M^*} - \Sigma_{M^*}(E)\,, \tag{26}$$

where $M^0_{M^*}$ is a bare mass and

$$\Sigma_{M^*}(E) = \sum_{cR,c'R'} \langle M^*|\Gamma_{M^*,cR} G_{cR,c'R'}(E) |\bar{\Gamma}_{c'R',M^*}\rangle. \tag{27}$$

Here $|\bar{\Gamma}_{c'R',M^*}\rangle$ is defined in Eq. (24).

The resonance pole positions, $E_{\rm pole}$, are defined as zeros of $G^{-1}_{M^*}(E)$. They are on the unphysical sheets of the complex-energy Riemann surface and are thus defined by the following equation:

$$G^{-1}_{M^*}(E_{\rm pole}) = 0. \tag{28}$$

We use the analytic continuation method of Refs. [47, 48] to solve Eq. (28) and find $E_{\rm pole}$ for the considered coupled-channels model with unstable meson-R channels.

If we replace the dressed vertex $|\bar{\Gamma}_{cR,M^*}\rangle$ by the bare vertex $\Gamma_{cR,M^*}|M^*\rangle$ in calculating $\Sigma_{M^*}(E_{\rm pole})$ of Eq. (27), then the solution of Eq. (28) is the pole position of the isobar model, which does not include the three-mesons final state interactions.

We now note that the Green function (26) can be related to the excitation of M^* in the $cR \to c'R'$ transition amplitude $T^{\rm res}_{c'R',cR}(E)$. The matrix element of Eq. (4) between $\langle c'R'|$ and $|cR\rangle$ states is

$$T_{c'R',cR}(E) = T'_{c'R',cR}(E) + T^{\rm res}_{c'R',cR}(E),$$

where the first term has been defined in Eq. (7). The second term is the "resonant" part, and is shown to be (using the projection operator methods)

$$T^{\rm res}_{c'R',cR}(E) = \frac{\langle c'R'|\bar{\Gamma}_{c'R',M^*}\rangle\langle\bar{\Gamma}_{M^*,cR}|cR\rangle}{E - M^0_{M^*} - \Sigma_{M^*}(E)}, \tag{29}$$

where

$$\langle\bar{\Gamma}_{M^*,cR}| = \sum_{c''R''}\langle M^*|\Gamma_{c''R'',M^*}\left[\delta_{c''R'',cR} + \sum_{c'''R'''}T'_{c''R'',c'''R'''}G_{c'''R''',cR}(E)\right]. \tag{30}$$

The self-energy $\Sigma_{M^*}(E)$ in Eq. (29) is defined in Eq. (27), and can be related to the decay amplitude [Eq. (14)] as follows. For a derivation, consult Appendix A. Consider the "decay" width $\Gamma^{M^*}_{\rm tot}(E)$ of the *bare* M^* (not the physical resonance state) defined by

$$\Gamma^{M^*}_{\rm tot}(E) = 2\pi\sum_{abc}\delta(E - E_a - E_b - E_c)|T_{abc,M^*}(E)|^2. \tag{31}$$

By using the unitarity relation for T' in Eq. (5), we can actually show that the right hand side of the above equation is

$$2\pi\sum_{abc}\delta(E - E_a - E_b - E_c)|T_{abc,M^*}(E)|^2 = -2{\rm Im}[\Sigma_{M^*}(E)]. \tag{32}$$

Equation (32) is used to check the accuracy of our numerical calculations of the Dalitz plots which are calculated from $T_{abc,M^*}(E)$ using the formula detailed in Appendix B.

III. FORMULA FOR NUMERICAL CALCULATIONS

For numerical calculations of decays of M^* into three light pseudoscalar mesons, $M^* \to abc$ (Fig. 2), we perform partial-wave expansions of the equations presented in Sec. II in the M^* rest frame. The kinematics of this decay is specified by the following:

$$\begin{aligned} M^*(\vec{0}, S^z_{M^*}, T^z_{M^*}) &\to R(\vec{p}_R, s^z_R, t^z_R) + c(\vec{p}_c, 0, t^z_c) \\ &\to a(\vec{p}_a, 0, t^z_a) + b(\vec{p}_b, 0, t^z_b) + c(\vec{p}_c, 0, t^z_c), \end{aligned} \tag{33}$$

where the variables in the parenthesis for each particle are its momentum, z-components of the spin and isospin, respectively.

Our task in this section is to relate the partial-wave forms of all of the equations presented in Sec. II to the basic input which will be determined by using the available empirical meson-meson scattering ($\pi\pi \to \pi\pi$, $\pi K \to \pi K$, etc) amplitudes. In this way, the final three-meson scattering effects can be predicted for investigating heavy meson decays.

A. $R \to ab$ decays

In a decay $R \to ab$, the spin (s_R) [isospin (t_R)] of the parent R state is same as the relative orbital angular momentum L_{ab} [total isospin I_{ab}] of the two-body ab system. Thus the partial-wave expansion of the vertex function $f_{ab,R}$ in the rest frame of R is

$$f_{ab,R}(\vec{q}) = \langle t_a\, t_a^z\, t_b\, t_b^z | t_R\, t_R^z \rangle Y_{s_R, s_R^z}(\hat{q})\, \tilde{f}_{ab,R}^{L_{ab} I_{ab}}(q). \tag{34}$$

Here t_a is the isospin of meson a and t_a^z is its z-component; $\langle j_1 m_1 j_2 m_2 | JM \rangle$ is the Clebsch-Gordan coefficient; $\vec{q}$ is the relative momentum between a and b; $\tilde{f}_{ab,R}^{L_{ab} I_{ab}}(q)$ is a scalar function satisfying $\tilde{f}_{ab,R}^{L_{ab} I_{ab}}(q) = 0$ for $L_{ab} \neq s_R$ and $I_{ab} \neq t_R$.

We use the parametrization

$$\tilde{f}_{ab,R}^{L_{ab} I_{ab}}(q) = \delta_{s_R, L_{ab}} \delta_{t_R, I_{ab}} \frac{g_{ab,R}}{\sqrt{m_\pi}} \left[\frac{1}{1 + (q/c_{ab,R})^2} \right]^{1 + (L_{ab}/2)} \left(\frac{q}{m_\pi} \right)^{L_{ab}}. \tag{35}$$

The parameters $g_{ab,R}$ and $c_{ab,R}$ and the bare mass m_R of R are adjusted to fit the empirical partial-wave amplitudes. The number of bare R states included in the model depends on a partial wave considered and the energy region covered in the fit.

B. The $\pi\pi$ model

We give an expression for the amplitudes of the scattering of two light pseudoscalar mesons in the partial wave basis. Here we limit ourselves to only $\pi\pi$ scattering because we consider only three-pion heavy-meson decays in this work. To fit $\pi\pi$ data up to invariant mass $W = 2$ GeV, we include $\pi\pi$ and $K\bar{K}$ channels. Then Eq. (12) with total angular momentum L and total isospin I in each partial-wave is of the following analytic form [Note that $\tilde{f}_{R,ab}^{L_{ab} I_{ab}}(q) = \tilde{f}_{ab,R}^{L_{ab} I_{ab} *}(q)$.]:

$$T_{\pi\pi,\pi\pi}^{LI}(q', q; E) = \sum_{R',R} \bar{f}_{\pi\pi,R'}^{LI}(q') \tau_{R',R}^{LI}(E) \bar{f}_{R,\pi\pi}^{LI}(q), \tag{36}$$

with

$$[(\tau^{LI})^{-1}(E)]_{R'R} = (E - m_R)\delta_{R',R} - \Sigma_{R',R}^{LI}(E), \tag{37}$$

where m_R is the bare mass of R and

$$\Sigma_{R',R}^{LI}(E) = \sum_{ab=\pi\pi, K\bar{K}} \int_0^\infty q^2 dq \frac{\bar{f}_{R',ab}^{LI}(q) \bar{f}_{ab,R}^{LI}(q)}{E - E_a(q) - E_b(q) + i\epsilon}, \tag{38}$$

and

$$\bar{f}^{L_{ab},I_{ab}}_{ab,R}(q) = \begin{cases} \frac{1}{\sqrt{2}}\tilde{f}^{L_{ab},I_{ab}}_{ab,R}(q) & \text{(if } a \text{ and } b \text{ are identical particles),} \\ \tilde{f}^{L_{ab},I_{ab}}_{ab,R}(q) & \text{(otherwise).} \end{cases} \tag{39}$$

C. Coupled-channels equations for $cR \to c'R'$ scattering

For given total angular momentum J, parity P, and total isospin T, the partial-wave form of Eq. (7) for the $cR \to c'R'$ scattering can be written as

$$\begin{aligned} T'^{JPT}_{(c'R')_{l'},(cR)_l}(p',p;E) &= Z^{JPT}_{(c'R')_{l'},(cR)_l}(p',p;E) \\ &+ \sum_{(c'''R''')_{l'''},(c''R'')_{l''}} \int_0^\infty q^2 dq Z^{JPT}_{(c'R')_{l'},(c'''R''')_{l'''}}(p',q;E) G_{(c'''R''')_{l'''},(c''R'')_{l''}}(q,E) \\ &\times T'^{JPT}_{(c''R'')_{l''},(cR)_l}(q,p;E). \end{aligned} \tag{40}$$

Here $(cR)_l$ denotes the cR state with the relative angular momentum l allowed for given JPT; p (p') is the magnitude of the incoming (outgoing) relative momentum of the cR ($c'R'$) state. The Green function can be written as

$$\begin{aligned} [G^{-1}(q,E)]_{(c'''R''')_{l'''},(c''R'')_{l''}} = \delta_{l''',l''}\delta_{c''',c''}\{[E - E_{c''}(q) - E_{R''}(q)]\delta_{R''',R''} \\ -\Sigma^{c''}_{R''',R''}(q, E - E_{c''}(q))\}, \end{aligned} \tag{41}$$

where the self-energy $\Sigma^c_{R',R}(q,w)$ is calculated from Eq. (11) by inserting the partial-wave expansion (34) and performing a Lorentz transformation to boost the function $\tilde{f}^{L_{ab}I_{ab}}_{ab,R}(q)$ from the rest frame of R to the center of mass frame of cR system. We also need to symmetrize the intermediate states with identical mesons. Explicitly, we have

$$\Sigma^c_{R'R}(p,E) = \sum_{ab} \sqrt{\frac{m_{R'}m_R}{E_{R'}(p)E_R(p)}} \int_0^\infty q^2 dq \frac{M_{ab}(q)}{[M^2_{ab}(q)+p^2]^{1/2}} \frac{\bar{f}^{L_{ab}I_{ab}}_{R',ab}(q)\bar{f}^{L_{ab}I_{ab}}_{ab,R}(q)}{E - E_c(p) - [M^2_{ab}(q)+p^2]^{1/2} + i\epsilon}, \tag{42}$$

where the summation is over all two-mesons states ab of $R \to ab$ decay, $M_{ab}(q) = E_a(q) + E_b(q)$. The partial-wave matrix elements $Z^{JPT}_{(c'R')_{l'},(cR)_l}(p',p;E)$ in Eq. (40) of the Z-diagram mechanisms, defined by Eq. (9), are given in Appendix C for the case that R decays into two pseudo-scalar mesons.

D. The $M^* \to abc$ decay amplitudes

The amplitude [Eq. (23)] for a strong three-mesons decay is given by

$$T_{(ab)c,M^*}(\vec{p}_a,\vec{p}_b,\vec{p}_c;E) = \sum_{R'R} f_{ab,R'}(\vec{p}_a,\vec{p}_b) G_{cR',cR}(p_c,E) \bar{\Gamma}_{cR,M^*}(\vec{p}_c,E), \tag{43}$$

where the Green function $G_{cR',cR}$ has been defined by Eqs. (41) and (42).

The $R \to ab$ vertex function in Eq. (43) is obtained from boosting the matrix element $f_{ab,R}^{L_{ab}I_{ab}}(\vec{q})$, defined by Eq. (34) in the rest frame of R, to a moving frame where $\vec{p}_R = \vec{p}_a + \vec{p}_b$:

$$f_{ab,R}(\vec{p}_a,\vec{p}_b) = \sqrt{\frac{m_R E_a(q) E_b(q)}{E_R(p_R) E_a(p_a) E_b(p_b)}} \langle t_a t_a^z t_b t_b^z | t_R t_R^z \rangle Y_{s_R,s_R^z}(\hat{q}) \tilde{f}_{ab,R}^{L_{ab}I_{ab}}(q), \tag{44}$$

where $\vec{q}$ is the relative momentum between a and b in their center of mass system; the relation among $\vec{q}$, $\vec{p}_a$ and $\vec{p}_b$ can be seen in Appendix C [Eqs. (C5) and (C6)]. For the strong decays, $\bar{\Gamma}_{cR,M^*}$ in Eq. (43) for the dressed $M^* \to cR$ vertex can be written down by using Eq. (24) as

$$\bar{\Gamma}_{cR,M^*}(\vec{p}_c,E) = \sum_{l,l^z,s_R^z} \sum_{t_R^z,t_c^z} \langle l l^z s_R s_R^z | S_{M^*} S_{M^*}^z \rangle \langle t_R t_R^z t_c t_c^z | T_{M^*} T_{M^*}^z \rangle Y_{l,l^z}(-\hat{p}_c) \bar{F}_{(cR)_l,M^*}(p_c,E), \tag{45}$$

where S_{M^*} and T_{M^*} are the spin and isospin of M^*, and (denoting the parity of M^* as P_{M^*})

$$\bar{F}_{(cR)_l,M^*}(p_c,E) = F_{(cR)_l,M^*}(p_c) + \sum_{(c''R'')_{l''},(c'R')_{l'}} \int_0^\infty dq\, q^2 T'^{S_{M^*}P_{M^*}T_{M^*}}_{(cR)_l,(c''R'')_{l''}}(p_c,q;E) \times G_{(c''R'')_{l''},(c'R')_{l'}}(q,E) F_{(c'R')_{l'},M^*}(q). \tag{46}$$

We parametrize the bare vertex function $F_{(cR)_l,M^*}(p)$ as

$$F_{(cR)_l,M^*}(p) = \frac{1}{(2\pi)^{3/2}} \frac{C_{(cR)_l,M^*}}{\sqrt{\Lambda_0}} \left(\frac{\Lambda_{(cR)_l,M^*}^2}{p^2 + \Lambda_{(cR)_l,M^*}^2} \right)^{2+(l/2)} \left(\frac{p}{m_\pi} \right)^l, \tag{47}$$

where $C_{(cR)_l,M^*}$, $\Lambda_{(cR)_l,M^*}$ and m_π are the coupling, cutoff and the pion mass, respectively; Λ_0 is a scale factor, and is set to be $\Lambda_0 = 1$ GeV. The couplings $C_{(cR)_l,M^*}$ are non-zero only when the transition $M^* \to (cR)_l$ is allowed by symmetries, e.g., those are non-zero only when l satisfies $|S_{M^*} - s_R| \le l \le S_{M^*} + s_R$ and $P_{M^*} = P_R \times (-)^{l+1}$. Here it is noted that for a strong decay the bare vertex function $F_{(cR)_l,M^*}(p)$ is related with Γ_{cR,M^*} as

$$\Gamma_{cR,M^*}(\vec{p}) = \sum_l \langle t_c t_c^z t_R t_R^z | T_{M^*}, t_R^z + t_c^z \rangle \langle l l^z s_R s_R^z | S_{M^*}, l^z + s_R^z \rangle Y_{l,l^z}(-\hat{p}) F_{(cR)_l,M^*}(p). \tag{48}$$

For describing the weak decays of M^* such as D^0, the above expressions of the $M^* \to cR$ vertex function need to be modified to include the isospin non-conserving $\Delta T \neq 0$ transition. This will not be considered here. Instead, we are only interested in the importance of three-meson scattering after the weak decay of D^0, and it is sufficient to use the above parametrization by extending $F_{(cR)_l,M^*}$ in Eq. (47) to depend on JPT of cR state.

The amplitude for the commonly used isobar model, as defined by Eq. (21), is

$$T^{\rm Isobar}_{(ab)c,M^*}(\vec{p}_a,\vec{p}_b,\vec{p}_c;E) = \sum_{R'R} f_{ab,R'}(\vec{p}_a,\vec{p}_b) G_{cR',cR}(p_c,E)\Gamma_{cR,M^*}(\vec{p}_c). \tag{49}$$

We see from Eqs. (43) and (49) that three-mesons decay amplitudes of these two models differ from each other only in the functions describing the $M^* \to cR$ decay. The formulae for calculating the Dalitz plots of final three-meson distributions from these decay amplitudes [Eqs. (43) and (49)] are given in Appendix B.

E. Determinations of resonance positions

With the partial-wave expansion (45), the resonance pole condition $G^{-1}_{M^*}(E_{\rm pole}) = 0$ of Eq. (28) leads to

$$E_{\rm pole} = M^0_{M^*} + \Sigma_{M^*}(E_{\rm pole}), \tag{50}$$

where [Note that $F_{M^*,(c'R')_{l'}}(q) = F^*_{(c'R')_{l'},M^*}(q)$.]

$$\Sigma_{M^*}(E) = \sum_{(c'R')_{l'},(cR)_l} \int_C dq q^2 F_{M^*,(c'R')_{l'}}(q) G_{(c'R')_{l'},(cR)_l}(q,E) \bar{F}_{(cR)_l,M^*}(q,E). \tag{51}$$

Here $\bar{F}_{(cR)_l,M^*}(q,E)$ has been defined by Eq. (46); $\int_C dq$ means the momentum integral is performed along the complex momentum path C.

We apply the analytic continuation method developed in Refs. [47, 48] to find resonance poles from solving Eqs. (50) and (51) for the considered model.

F. Relations of the isobar models with the Breit-Wigner parametrization

For the isobar model defined within our formulation, we can establish some relations with the commonly used Breit-Wigner parametrization. If we neglect the Z-diagram effects by

setting $\bar{F}_{(cR)_l,M^*}$ to $F_{(cR)_l,M^*}$ and use the partial-wave expansion (45), Eq. (29) for $cR \to c'R'$ scattering can be written as (omitting the momentum variables)

$$T^{\mathrm{res},JPT}_{(c'R')_{l'},(cR)_l}(E) \to \frac{F_{(c'R')_{l'},M^*}F_{M^*,(cR)_l}}{E - M^0_{M^*} - \Sigma^{(0)}_{M^*}(E)}, \tag{52}$$

where $J = S_{M^*}$, $P = P_{M^*}$, $T = T_{M^*}$ for strong decays, and

$$\Sigma^{(0)}_{M^*}(E) = \sum_{(c'R')_{l'},(cR)_l} \int_0^\infty q^2 dq F_{M^*,(c'R')_{l'}}(q) G_{(c'R')_{l'},(cR)_l}(q,E) F_{(cR)_l,M^*}(q). \tag{53}$$

Equation (52) is similar to that of the commonly used Breit-Wigner parametrization in the analysis using the isobar model or the K-matrix model:

$$T^{\mathrm{BW},JPT}_{(c'R')_{l'},(cR)_l}(E) = \frac{[e^{i\delta_{(c'R')_{l'}}}\sqrt{\Gamma^{\mathrm{BW}}_{(c'R')_{l'}}/2}][e^{i\delta_{(cR)_l}}\sqrt{\Gamma^{\mathrm{BW}}_{(cR)_l}/2}]}{E - M^{\mathrm{BW}}_r + i(\Gamma^{\mathrm{BW}}_{\mathrm{tot}}/2)}, \tag{54}$$

where $\Gamma^{\mathrm{BW}}_{(cR)_l}$ is a partial decay width for $M^* \to (cR)_l$, which is related to the total decay width as

$$\Gamma^{\mathrm{BW}}_{\mathrm{tot}} = \sum_{(cR)_l} \Gamma^{\mathrm{BW}}_{(cR)_l}. \tag{55}$$

Now we introduce $\bar{s}_R$ and $\bar{t}_R$ that specify the spin and isospin of R. Then Eq. (53) can be written as

$$\Sigma^{(0)}_{M^*}(E) = \sum_{\bar{s}_R,\bar{t}_R} \left[\Sigma^{(0)}_{M^*}(E)\right]_{\bar{s}_R,\bar{t}_R}, \tag{56}$$

where

$$\left[\Sigma^{(0)}_{M^*}(E)\right]_{\bar{s}_R,\bar{t}_R} = \sum_{\{(c'R')_{l'}|s_{R'}=\bar{s}_R,t_{R'}=\bar{t}_R\}} \sum_{\{(cR)_l|s_R=\bar{s}_R,t_R=\bar{t}_R\}} \times \int_0^\infty q^2 dq F_{M^*,(c'R')_{l'}}(q) G_{(c'R')_{l'},(cR)_l}(q,E) F_{(cR)_l,M^*}(q). \tag{57}$$

We denote a conditional sum of $(cR)_l$ by $\sum_{\{(cR)_l|s_R=\bar{s}_R,t_R=\bar{t}_R\}}$, in which the $(cR)_l$ state is summed, keeping s_R and t_R constant, i.e., $s_R = \bar{s}_R$ and $t_R = \bar{t}_R$. Thus it is reasonable to make the following interpretations

$$M^{\mathrm{BW}}_r = M^0_{M^*} + \mathrm{Re}\left[\Sigma^{(0)}_{M^*}(M^{\mathrm{BW}}_r)\right], \tag{58}$$

$$\Gamma^{\mathrm{BW}}_{\mathrm{tot}}(M^{\mathrm{BW}}_r) = -2\mathrm{Im}\left[\Sigma^{(0)}_{M^*}(M^{\mathrm{BW}}_r)\right], \tag{59}$$

$$\Gamma^{\mathrm{BW}}_{\bar{s}_R,\bar{t}_R}(M^{\mathrm{BW}}_r) = -2\mathrm{Im}\left[[\Sigma^{(0)}_{M^*}(M^{\mathrm{BW}}_r)]_{\bar{s}_R,\bar{t}_R}\right]. \tag{60}$$

Equations (58)-(60) will be used in our later comparisons with the data listed by PDG. We note here that the above identifications are very qualitative.

IV. APPLICATION

In this section, we apply our model explained in the previous sections to investigate the three-pions decays of heavy mesons $a_1(1260)$, $\pi_2(1670)$, $\pi_2(2100)$, and also D^0. Our first task is to determine the parameters of our model. To simplify the calculations, we determine the vertex interactions $R \to ab$ for $ab = \pi\pi, K\bar{K}$ by fitting only the $\pi\pi$ scattering phase shifts up to the invariant mass $W = 2000$ MeV. This is clearly a simplification since the data associated with $K\bar{K}$ channel should in principle be included in our fits and we must also include four-pions channels which have been considered to be important in the isoscalar-scalar ($L = I = 0$) partial wave. However, such a detailed study of meson-meson scattering can only be done rigorously by extending our formulation to account for the direct meson-meson interactions $v_{a'b',ab}$ which must be carefully derived from effective field theory approaches, e.g., Refs. [49–52], to make sure that the predicted $\pi\pi$ amplitudes near threshold have the analytic properties constrained by the chiral symmetry. Furthermore, the inclusion of $v_{a'b',ab}$ in our model Hamiltonian H'' of Eq. (3) will greatly complicate the scattering formulation, as can be seen in the $\pi\pi N$ formulation presented in Ref. [39]. For our present limited purpose of demonstrating the importance of three-body unitarity, our simplified model which reproduces $\pi\pi$ phase shifts in s, p and d waves up to $W = 2000$ MeV is sufficient. For the same reasons, we neither include $\pi K\bar{K}$ Z-diagrams nor make an attempt to estimate the errors of the determined parameters.

In Sec. IV A, we determine the model parameters by fitting the $\pi\pi$ phase shifts and resonance parameters listed in PDG. With the parameters obtained from the fit, we determine the pole positions (Sec. IV B) and calculate the Dalitz plots (Sec. IV C) from the $M^* \to \pi\pi\pi$ amplitudes including the Z-diagram [Eq. (43)] or without the Z-diagram [Eq. (49)] with the formula given in Appendix A. For the calculation without the Z-diagram, we either simply turn off the Z-diagram in the full calculation, or fit the isobar model to the Dalitz plot from the full calculation. Our main focus is to examine the effect of the Z-diagram (and thus the three-body unitarity) on these quantities by detailed comparison of the results calculated with and without Z-diagram mechanisms, thereby providing information about the extent to which the commonly used isobar model analysis is valid for extracting the properties of heavy meson from three-mesons decay data.

TABLE I. Masses (M_{R_i}), couplings ($g_{\pi\pi,R_i}$, $g_{K\bar{K},R_i}$), and cutoffs ($c_{\pi\pi,R_i}$, $c_{K\bar{K},R_i}$) of the i-th bare R states, R_i, in the $\pi\pi$ partial wave with the angular momentum L and the isospin I. The couplings and cutoffs are defined in Eq. (35).

R (L,I)	M_{R_1} (MeV)	$g_{\pi\pi,R_1}$	$c_{\pi\pi,R_1}$ (MeV)	$g_{K\bar{K},R_1}$	$c_{K\bar{K},R_1}$ (MeV)	M_{R_2} (MeV)	$g_{\pi\pi,R_2}$	$c_{\pi\pi,R_2}$ (MeV)	$g_{K\bar{K},R_2}$	$c_{K\bar{K},R_2}$ (MeV)
f_0 (0, 0)	1220	−0.898	441	0.008	1970	2400	0.495	955	−1.179	394
ρ (1, 1)	891	−0.291	394	0.150	467	1840	0.015	1973	0.167	394
f_2 (2, 0)	1607	−0.051	567	0.021	818	—	—	—	—	—

A. Determinations of model parameters

1. *Fits to $\pi\pi$ amplitudes*

Our first task is to determine the $R \to ab$ vertex function $\tilde{f}_{ab,R}^{L_{ab}I_{ab}}(q)$, defined by Eq. (34), by fitting the $\pi\pi$ phase shifts. We include $\pi\pi$ and $K\bar{K}$ channels and use the formulae (35) and (36) to fit the available $\pi\pi$ amplitude in s, p and d partial waves. In our fits, the number of bare R included in each partial wave is 2, 2, 1 for $(s_R, t_R) = (L_{ab}, I_{ab}) = (0,0), (1,1), (2,0)$, respectively. The resulting parameters are listed in Table I.

As shown in Fig. 3, we are able to get good fits to the empirical partial-wave amplitudes [53–55]. The non-zero values of the inelasticities are due to the couplings to $K\bar{K}$ channels. For s and p waves, $(L_{ab}, I_{ab}) = (0,0), (1,1)$, the high quality fits are obtained only when two bare R states are included. It is noted that a partial wave analysis using more recent data [56] has found a unique solution for $W \sim$ 1000-1800 MeV. Although our present model is reasonable enough to address the question on the importance of the Z-graphs, those data should be considered for a more quantitative application of our model.

We have also determined the resonance pole positions by applying the analytic continuation method of Refs. [47, 48]. The results for $\mathrm{Re}\,[E] \leq 2$ GeV are listed in Table II. It is interesting to note that we have two bare R states in s-wave, but we have identified three resonance poles on different sheets of Riemann surface: sheet II is (up) consisting of the unphysical (u) $\pi\pi$ and physical (p) $K\bar{K}$ sheet, and sheet III is (uu).

We find that the poles listed in Table II can be identified with the $\pi\pi$ resonances listed

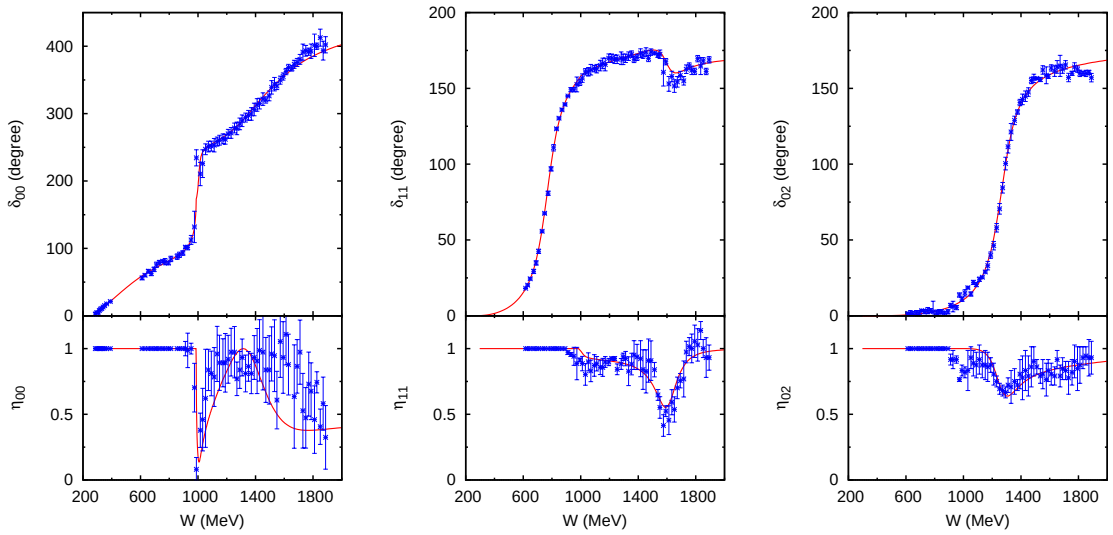

FIG. 3. (Color online) Phase shifts (upper) and inelasticities of the $\pi\pi$ scattering (lower): (left panels) $L = I = 0$, (center panels) $L = I = 1$, and (right panels) $L = 2, I = 0$. Data are taken from Ref. [53–55].

TABLE II. Pole positions of the $\pi\pi$ partial wave amplitudes with the angular momentum L and the isospin I in the complex energy plane. We list only the poles below Re$[E] \leq 2$ GeV. Roman numbers in the square brackets specify the Riemann sheet on which the pole exists. We use the convention for specifying each Riemann sheet, I – IV, which is defined in, e.g., Ref. [57].

L	I	Pole positions (GeV) [Riemann sheet]		
0	0	$0.43 - 0.27i$ [II]	$1.00 - 0.009i$ [II]	$1.35 - 0.17i$ [III]
1	1	$0.77 - 0.081i$ [II]	$1.61 - 0.12i$ [III]	—
2	0	$1.25 - 0.10i$ [III]	—	—

by PDG [58]. For the $(L, I) = (0, 0)$ s-wave partial wave, our results can be identified with $f_0(600)$ (or σ), $f_0(980)$ and $f_0(1370)$. For $(L, I) = (1, 1)$ p wave, our results correspond to the $\rho(770)$ and a higher mass ρ. The resonance $f_2(1270)$ can be identified with our results for the $(L, I) = (0, 2)$ d-wave partial waves. Here we note that the imaginary part of the position $(1.00 - 0.009i)$ GeV, which corresponds to having 18 MeV of the full width, in the isoscalar-scalar $L = I = 0$ partial wave (the first row of Table II) is too small compared with the full width $40 - 100$ MeV of $f_0(980)$ listed by PDG. This perhaps can be improved only by extending our model to include four-pions channel and direct interactions $v_{ab,a'b'}$

with $ab, a'b' = \pi\pi, K\bar{K}$. But this is beyond the scope of this investigation, as discussed in the beginning of Sec. IV. Here we mention that the imaginary parts of the pole position of $f_0(980)$ from some previous $\pi\pi$ models are also smaller than the full width, (40-100) MeV, listed by PDG, such as 28 MeV from Ref. [59], and 29 MeV from Ref. [60]. A quark model [61] also gave only 15 MeV for the width of $f_0(980)$.

In most of the previous studies of heavy meson decays, only the s-wave resonances are included as resonance poles while the p-wave poles are included in Ref. [9]. The other resonances are included using the Breit-Wigner form. In our calculations we include all resonances poles in $\pi\pi$ s, p and d partial waves listed in Table II.

We evaluate the πR Green functions [Eq. (41)] and the matrix elements of Z-diagrams [Eq. (C10)] with the parameters listed in Table I. We solve the coupled-channels equations (40) to obtain the $\pi R \to \pi R'$ scattering amplitude for given (J, P, T), $T^{JPT}_{(\pi R')_{l'},(\pi R)_l}(p', p, E)$, including all allowed relative orbital angular momentum between π and R. The resulting $T^{JPT}_{(\pi R')_{l'},(\pi R)_l}(p', p, E)$ are then used to calculate the $M^* \to \pi\pi\pi$ decay amplitudes (43) and find resonance poles associated with M^* by solving Eqs. (50) and (51).

2. Parameters for the decays of M^* states

To calculate the decay amplitudes for $a_1(1260)$, $\pi_2(1670)$, $\pi_2(2100)$ and D^0, we now need to determine their bare masses $M^0_{M^*}$, and the parameters $C_{(\pi R)_l,M^*}$, $\Lambda_{(\pi R)_l,M^*}$ of Eq. (47) for the $M^* \to \pi R$ vertex functions. Ideally, we should determine these parameters by fitting the Dalitz plots of $\pi\pi\pi$ distributions measured experimentally. However, such a rather complex process is not needed for our limited purpose here to mainly investigate the extent to which the commonly used isobar model analysis is valid. It is sufficient to choose our parameters guided by the resonance positions and branching ratios listed by PDG [58][1]. The data for the resonances considered in this work are listed in Table III.

We first notice that the data in Table III are the averaged values from several analyses. Most of these analyses parametrized the M^* decay amplitudes with the Breit-Wigner form, and all of them treated the final three pions as the paired two pions (whose correlations are described by either the Breit-Wigner form or the K-matrix) and the non-interacting

[1] We do not use data from PDG directly, because some channels, which have small but non-zero branching ratios, are not included in our model.

TABLE III. Properties of $M^* = a_1(1260),\ \pi_2(1670),\ \pi_2(2100)$ to which our model is fitted: Isospin (I), spin (J), parity (P), and charge conjugation parity (C); pole masses ; branching ratios (BR).

	$a_1(1260)$	$\pi_2(1670)$	$\pi_2(2100)$
$I(J^{PC})$	$1(1^{++})$	$1(2^{-+})$	$1(2^{-+})$
Pole masses (MeV)	$1230 - 213i$	$1672 - 130i$	$2090 - 313i$
$\mathrm{BR}(M^* \to \pi f_0)$ (%)	23	13	45
$\mathrm{BR}(M^* \to \pi\rho)$ (%)	74	31	19
$\mathrm{BR}(M^* \to \pi f_2)$ (%)	2.5	56	35

spectator. We thus assume that the $\Gamma^{\rm BW}_{\rm tot}/2$ is the imaginary part of the pole masses in Table III, from which we can use the listed branching ratios $\mathrm{BR}(M^* \to cR)$ to calculate $\Gamma^{\rm BW}_{cR} = \mathrm{BR}(M^* \to cR) \times \Gamma^{\rm BW}_{\rm tot}$.[2] The resulting values of $\Gamma^{\rm BW}_{cR}$ as well as the pole masses of M^* are then used as data to determine the parameters of $F_{(cR)_l,M^*}(p)$ [Eq. (47)] and $M^0_{M^*}$ [Eq. (26)] by using Eqs. (50), (59) and (60). Because we have more parameters than the number of data, we use for simplicity the same cutoff for all of $F_{(cR)_l,M^*}(p)$ for a given M^*, and we only adjust the coupling constant $C_{(cR)_{l\rm min},M^*}$ with the lowest allowed angular momentum $l_{\rm min}$ for cR; the other $C_{(cR)_l,M^*}$ are set to zero. The resulting parameters for $a_1(1260)$, $\pi_2(1670)$, and $\pi_2(2100)$ are listed in Tables IV-VI.

The D^0 meson (1865 MeV, $J^P = 0^-$) mainly decays weakly and thus three-meson scattering effects have very little effects on its mass and width. We thus will only investigate the Dalitz plot for the $D^0 \to \pi^+\pi^-\pi^0$ decay. The BABAR collaboration [19] presented the Dalitz plot data for this process, and we utilize their observation that the $D^0 \to \pi^+\pi^-\pi^0$ decay is dominated by $T = 0$ $\pi\rho$ channel for simplicity. Thus we use the following parameters: $C_{(\pi\ 1{\rm st}\rho)_1,M^*} = 1$, and $C_{(cR)_l,M^*} = 0$ for other partial waves; $\Lambda_{cR,M^*} = 1$ GeV. We are only interested in the difference between the Dalitz plots calculated with and without Z-diagram, so this simple choice of parameters is sufficient. It turns out that this simple choice of the parameters well reproduces the shape of the Dalitz plot presented by the BABAR collaboration [19]. Clearly, the above procedure is just for a very rough estimate of bare M^* parameters. In the future, we should fit the Dalitz plot data directly. But the present

[2] In data analyses with the Breit-Wigner parametrization of the M^* decay amplitudes, the partial width and the imaginary part of the M^* pole masses are not related by $\Gamma^{\rm BW}_{cR} = \mathrm{BR}(M^* \to cR) \times \Gamma^{\rm BW}_{\rm tot}$. We use this relation just for determining the parameters with this rough estimate.

TABLE IV. Masses ($M^0_{M^*}$), cutoffs ($\Lambda_{\pi R,M^*}$), and couplings ($C_{(\pi R_i^{LI})_l,M^*}$) of the bare $M^* = a_1(1260)$. The cutoffs and couplings are defined in Eq. (47). For $C_{(\pi R_i^{LI})_l,M^*}$, R_i^{LI} means the i-th bare R state with the spin L and the isospin I, and l denotes the orbital angular momentum between R_i^{LI} and π. The second and third columns show the parameters for the unitary (isobar-fit) model. The hyphens (—) indicate the unused parameters. See the text for the definition of the isobar-fit model.

	$a_1(1260)$	
	Unitary model	Isobar-fit model
$M^0_{M^*}$ (MeV)	1687	1901
$\Lambda_{\pi R,M^*}$ (MeV)	832	1073
$C_{(\pi R_1^{00})_1,M^*}$	4.46	2.84
$C_{(\pi R_2^{00})_1,M^*}$	−3.41	−0.13
$C_{(\pi R_1^{11})_0,M^*}$	16.8	13.3
$C_{(\pi R_1^{11})_2,M^*}$	—	0.15
$C_{(\pi R_2^{11})_0,M^*}$	−0.76	−10.0
$C_{(\pi R_2^{11})_2,M^*}$	—	−0.17
$C_{(\pi R_1^{20})_1,M^*}$	10.4	7.37
$C_{(\pi R_1^{20})_3,M^*}$	—	−0.06

procedure is sufficient for our purpose in this paper.

B. Z-diagram effects on the pole positions of $a_1(1260)$, $\pi_2(1670)$, and $\pi_2(2100)$

In Sec. IV A 2, we solved Eqs. (50) and (51) to fit the pole positions for $a_1(1260)$, $\pi_2(1670)$ and $\pi_2(2100)$ listed in PDG. Our fitted values are shown in the row labeled as "with Z" of Table VII. When the Z-diagram mechanisms are turned off, which is achieved by replacing the dressed vertex function $\bar{F}_{(cR)_l,M^*}$ with the bare $F_{(cR)_l,M^*}$ in calculating $\Sigma_{M^*}(E)$ [Eq. (51)], the solution of Eq. (50) becomes the values shown in the row labeled as "without Z" of Table VII.

Comparing the two rows in Table VII, we see that the Z-diagram mechanisms can change the pole positions significantly. In particular, the imaginary parts can be changed by 65 MeV

TABLE V. Masses ($M^0_{M^*}$), cutoffs ($\Lambda_{\pi R,M^*}$), and couplings ($C_{(\pi R_i^{LI})_l,M^*}$) of the bare $M^* = \pi_2(1670)$. For the description of the table, see the caption of Table. IV.

	$\pi_2(1670)$	
	Unitary model	Isobar-fit model
$M^0_{M^*}$ (MeV)	1877	1912
$\Lambda_{\pi R,M^*}$ (MeV)	874	885
$C_{(\pi R_1^{00})_2,M^*}$	0.67	0.55
$C_{(\pi R_2^{00})_2,M^*}$	0.99	0.97
$C_{(\pi R_1^{11})_1,M^*}$	−2.21	−1.67
$C_{(\pi R_1^{11})_3,M^*}$	—	—
$C_{(\pi R_2^{11})_1,M^*}$	0.50	3.58
$C_{(\pi R_2^{11})_3,M^*}$	—	—
$C_{(\pi R_1^{20})_0,M^*}$	−12.2	−11.3
$C_{(\pi R_1^{20})_2,M^*}$	—	—
$C_{(\pi R_1^{20})_4,M^*}$	—	—

for $a_1(1260)$ and 85 MeV for $\pi_2(2100)$ Accordingly, we expect that the extracted residues will also be significantly changed. The extraction of the residues for unstable particle channels is non-trivial, and is still being investigated, as explained in Ref. [48]. We thus do not have results for the Z-diagram effects on the branching ratios in this work.

C. Z-diagram effects on Dalitz plots

1. $D^0 \to \pi^+\pi^-\pi^0$

As discussed in Sec. IV A 2, we only include the bare $D^0 \to \pi\rho$ vertex with ($J^P = 0^-, T = 0, l = 1$) in this calculation, as guided by the analysis by the BABAR collaboration [19]; the πf_0 and πf_2 channels are coupled only through the final state interaction. The Dalitz plot calculated from our unitary amplitude $T_{\pi^+\pi^-\pi^0,D^0}(E = M_{D^0} = 1865$ MeV) from using Eq. (43) is shown in Fig. 4 (left panel). With an overall normalization factor, the pattern of our Dalitz plot is similar to BABAR's data [19]. The sharp peaks (darker red) near the

TABLE VI. Masses ($M^0_{M^*}$), cutoffs ($\Lambda_{\pi R,M^*}$), and couplings ($C_{(\pi R_i^{LI})_l,M^*}$) of the bare $M^* = \pi_2(2100)$. For the description of the table, see the caption of Table. IV.

	$\pi_2(2100)$	
	Unitary model	Isobar-fit model
$M^0_{M^*}$ (MeV)	2189	2280
$\Lambda_{\pi R,M^*}$ (MeV)	876	970
$C_{(\pi R_1^{00})_2,M^*}$	-0.93	-0.70
$C_{(\pi R_2^{00})_2,M^*}$	-0.001	-0.34
$C_{(\pi R_1^{11})_1,M^*}$	2.45	1.65
$C_{(\pi R_1^{11})_3,M^*}$	—	—
$C_{(\pi R_2^{11})_1,M^*}$	0.51	0.41
$C_{(\pi R_2^{11})_3,M^*}$	—	—
$C_{(\pi R_1^{20})_0,M^*}$	-11.9	-10.1
$C_{(\pi R_1^{20})_2,M^*}$	—	—
$C_{(\pi R_1^{20})_4,M^*}$	—	—

TABLE VII. Pole masses of $a_1(1260)$, $\pi_2(1670)$ and $\pi_2(2100)$. Here "with Z" denotes the results of the full unitary model, while "without Z" denotes the results in which the Z-diagrams are turned off from the full unitary model.

	Pole masses (MeV)		
	$a_1(1260)$	$\pi_2(1670)$	$\pi_2(2100)$
with Z	$1230 - 213\ i$	$1672 - 130\ i$	$2090 - 313\ i$
without Z	$1122 - 148\ i$	$1661 - 127\ i$	$2044 - 398\ i$

edges of distributions are due to the formation of a ρ resonance during the 3-π propagation. The almost empty center part is due to the destructive interferences along the symmetry axes, supporting the assumption that the $T = 0$ $\pi\rho$ channel dominates the decay [62].

With the same parameters and overall normalization factor, we then calculate the Dalitz plot from $T^{\rm Isobar}_{\pi^+\pi^-\pi^0,D^0}(E)$ using Eq. (49) which does not include Z-diagram mechanisms; namely only keep the first term in Fig. 2. In the right panel of Fig. 4, we show the ratios

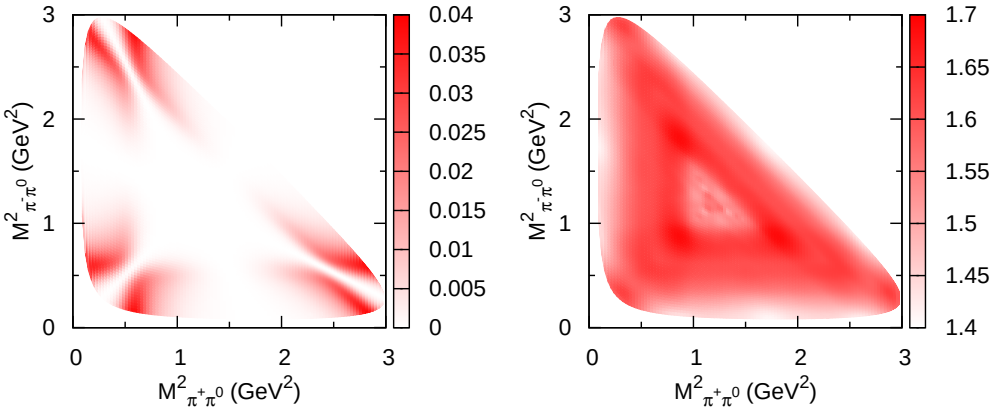

FIG. 4. (Color online) (left) Dalitz plot of $D^0 \to \pi^+\pi^-\pi^0$ decay; (right) Ratio of Dalitz plot distributions with and without the Z-graphs.

between the results obtained from calculations with and without the Z-diagram. Clearly, the Z-diagram mechanisms considerably change both the magnitudes and the shape of the Dalitz plot. In most of the area, the ratios (measured by the darkness as indicated on the right y-axis of the figure) are about 1.6. To see this more clearly, we show in Fig. 5 the double differential decay width distribution, $d^2\Gamma/(dM^2_{\pi^+\pi^0}dM^2_{\pi^-\pi^0})$ defined in Eq. (B2), at $M^2_{\pi^+\pi^0} = 0.3$ GeV^2. We see that at the ρ resonance peaks, the magnitudes can be enhanced by a factor of about 1.5 when Z-diagram mechanisms are included to satisfy the three-body unitarity.

Our results shown in Figs. 4 and 5 indicate the need to re-analyze the D meson decays data, with the three-body unitarity taken into account, to assess the results, such as CKM matrix elements, obtained with the isobar model analysis [18–23].

2. $a_1(1260), \pi_2(1670), \pi_2(2100) \to \pi^+\pi^-\pi^0$

The decays of these three mesons have been analyzed by using the isobar models. Our objective here is twofold. First we want to examine the Z-diagram effects on the Dalitz plots. Second, we regard the Dalitz plot generated from our unitary model [Eq. (43)] as the data, and fit them with the isobar model [Eq. (49)]. We refer to it as the isobar-fit model. In this way, we have the two models that reproduce the same Dalitz plot. However, the decay

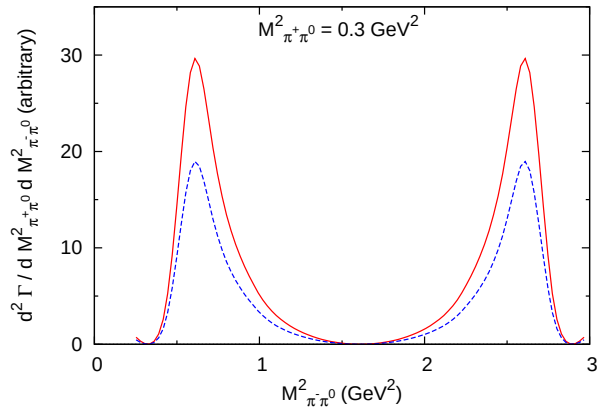

FIG. 5. (Color online) Double differential decay width distribution [Eq. (B2)] of $D^0 \to \pi^+\pi^-\pi^0$ decay at $M^2_{\pi^+\pi^0} = 0.3$ (GeV)^2. The red solid curve is from the full unitary model while the blue dashed curve is obtained by just turning off the Z-diagrams in the full model.

amplitudes from the two models are not necessarily the same, which we will examine. This examination is particularly interesting in the context of the extraction of the CKM phase γ from B and/or D decays. This is because the extracted γ depends on the decay amplitudes, particularly on its phase[3]. Thus the difference in the decay amplitude between our unitary model and the isobar-fit model does matter. We examine this for the strong decays of a_1 and π_2, which is suggestive enough for the extraction of γ with the isobar model analysis. Also, we study how well the three-body unitarity is satisfied in the isobar-fit model. Our unitary model satisfies it by definition (explicitly shown numerically later). A large violation of the unitarity raise a concern about the reliability in extracted quantities with the isobar model analysis.

We calculate the Dalitz plots at $E = \mathrm{Re}[M_R]$, for which we use M_R of the full model listed in Table VII. The results from our full model [using Eq. (43)] are shown in the left panels of Fig. 6 for $a_1(1260)$, Fig. 7 for $\pi_2(1670)$, and Fig. 8 for $\pi_2(2100)$. We see that they have rather complex structure. This is due to the resonances of $\pi\pi$ scattering implemented in the π-R Green function [Eq. (41)], and also interference among them as a consequence of summing coherently $\pi R \to \pi\pi\pi$ partial-wave amplitudes as calculated in Eq. (43). For

[3] There exists an alternative approach in which γ can be determined model-independently [63–65] solely from data, provided a large dataset is available. A feasibility study [65] showed that, with a dataset available near future, the precision of γ extracted with this approach is comparable to that obtained with the isobar model analysis. Future high statistic experiments (super B factory, LHCb) make this approach very interesting.

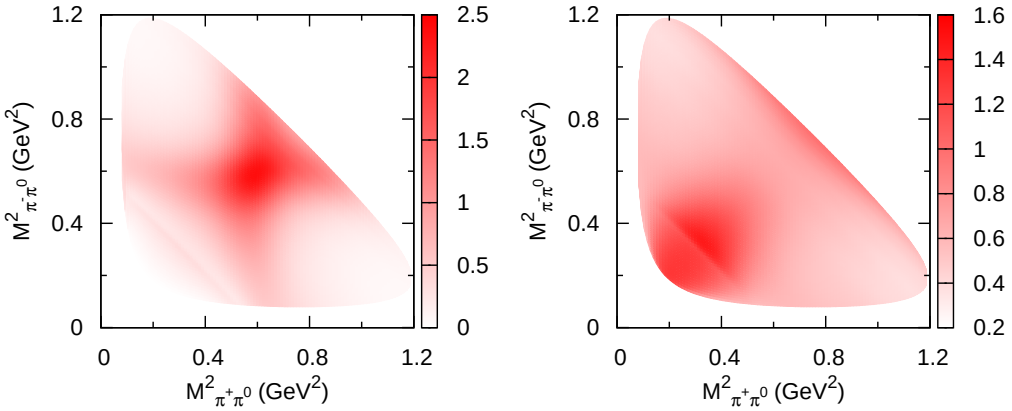

FIG. 6. (Color online) (left) Dalitz plot of $a_1(1260) \to \pi^+\pi^-\pi^0$; (right) Ratio of Dalitz plot distributions with and without the Z-graphs. The unit is GeV^{-3}.

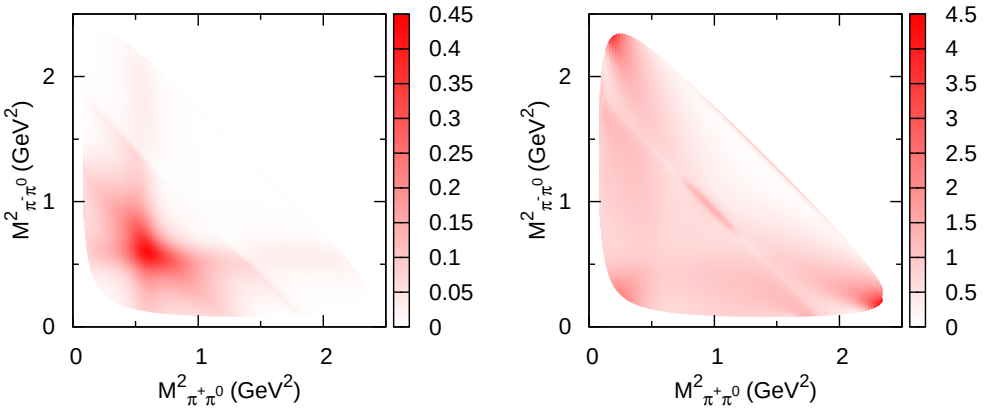

FIG. 7. (Color online) (left) Dalitz plot of $\pi_2(1670) \to \pi^+\pi^-\pi^0$; (right) Ratio of Dalitz plot distributions with and without the Z-graphs. The unit is GeV^{-3}.

example, two bands on $M^2_{\pi^+\pi^0} \sim 0.6$ GeV^2 and $M^2_{\pi^-\pi^0} \sim 0.6$ GeV^2 in Figs. 6-8 are due to the $\rho(770)$ resonance in the p-wave $\pi\pi$ scattering. A gap in $M^2_{\pi^+\pi^0} + M^2_{\pi^-\pi^0} \sim 0.6$ GeV^2 in Fig. 6 is due to the $f_0(980)$ resonance and opening of the $K\bar{K}$ channel. The Z-diagram effects are rather different in different parts of the Dalitz plots. This can be seen from the ratios between the Dalitz plots calculated with [Eq. (43)] and without [Eq. (49)] Z-diagram, as shown in the right hand sides of Figs. 6-8.

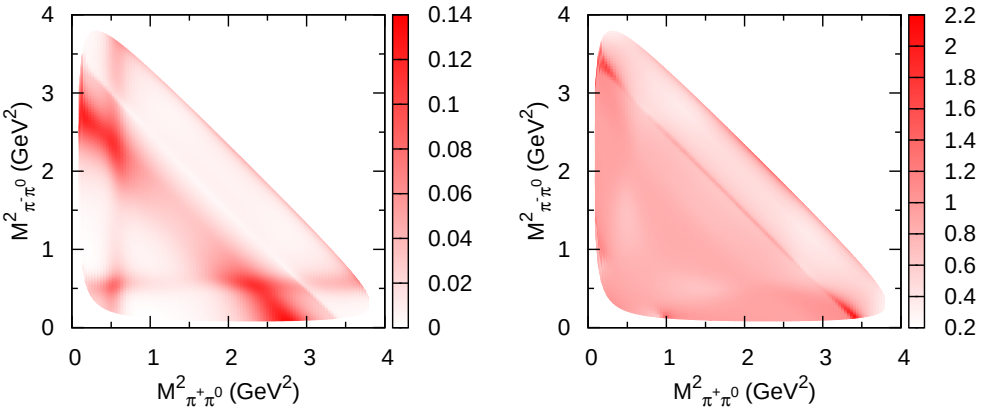

FIG. 8. (Color online) (left) Dalitz plot of $\pi_2(2100) \to \pi^+\pi^-\pi^0$; (right) Ratio of Dalitz plot distributions with and without the Z-graphs. The unit is GeV^{-3}.

To see the Z-diagram effects more clearly, we show in Fig. 9 the double differential decay width distributions [Eq. (B2)] for the decays of these three mesons at typical kinematics. By comparing the red solid curves and blue dashed curves, we see that the Z-diagram effects can significantly reduce the cross sections; in particular in the regions near the resonance peaks of $\pi\pi$ scattering.

Now we examine differences between the unitary and isobar models if both fit the same Dalitz plot. We treat the Dalitz plots in the left sides of Fig. 6-Fig. 8 as the data in fits using the isobar model [Eq. (49)] by adjusting the coupling constants, cutoffs of the vertex $F_{(cR)_l,M^*}$ of Eq. (47). In the fits, we assign either 5% error for each point of the Dalitz plot larger than 0.005 GeV^{-3}, or error of 0.005 GeV^{-3} otherwise. We are able to get reasonably good fits[4]. The resulting parameters for the isobar-fit model are rather different from the unitary model as shown in Tables IV-VI. The quality of our fits can be seen by comparing the dotted curves and the solid curves in Fig. 9. Accordingly, the decay widths to $\pi^+\pi^-\pi^0$ channel calculated from two models using Eq. (31) (keeping only $abc = \pi^+\pi^-\pi^0$) agree well, as seen in the third, fifth and seventh columns of Table VIII. However, we see in the second, fourth and sixth columns of Table VIII that the resonance pole positions from resulting

[4] In most Dalitz plot analysis with the isobar model, a (constant) nonresonant background amplitude with adjustable strength is included. Also, the $M^* \to \pi R$ couplings are in general complex in the isobar model in order to partially take account of the missing interaction between the spectator and the paired mesons. Because we obtained fits good enough for the following discussion, we do not include these degrees of freedom.

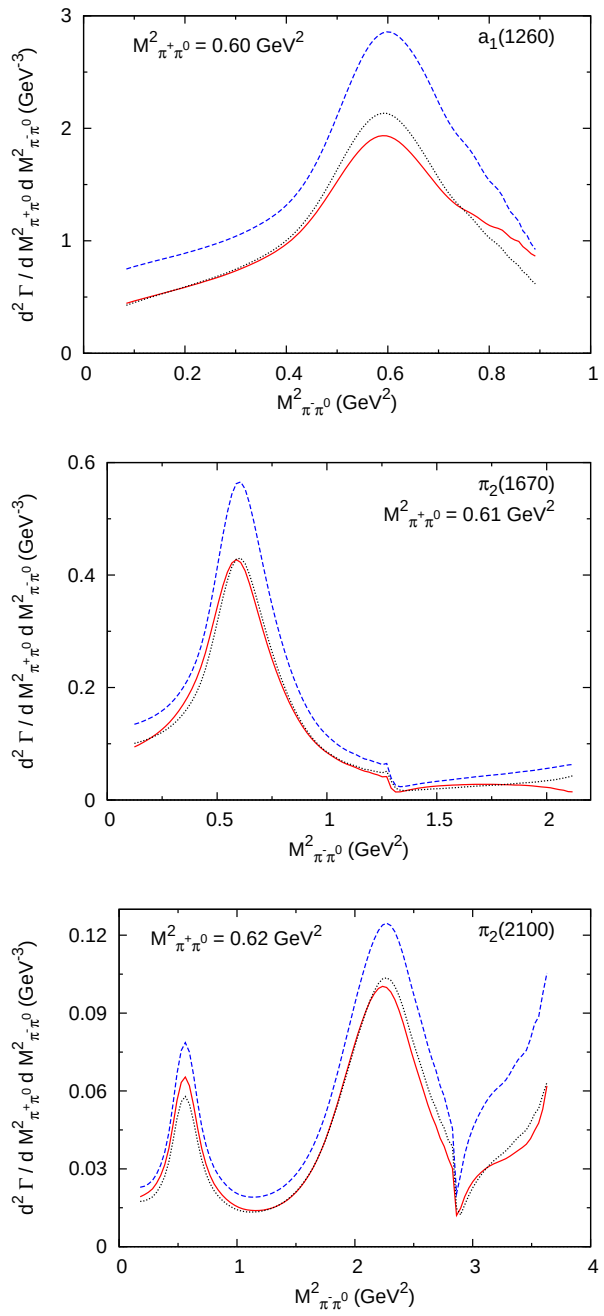

FIG. 9. (Color online) Double differential decay width distributions [Eq. (B2)] of $a_1(1260) \to \pi^+\pi^-\pi^0$ (top), $\pi_2(1670) \to \pi^+\pi^-\pi^0$ (middle), of $\pi_2(2100) \to \pi^+\pi^-\pi^0$ (bottom). The red solid curves are from the full unitary model while the blue dashed curves are obtained by just turning off the Z-diagrams in the full model. The black dotted curves are from the isobar-fit model (see the text for definition.).

TABLE VIII. The pole masses and total widths decaying to $\pi^-\pi^+\pi^0$ states ($\Gamma_{\pi^+\pi^-\pi^0}$) of $a_1(1260)$, $\pi_2(1670)$, and $\pi_2(2100)$. "Full" ("Isobar fit") is the results of the full unitary (isobar fit) model.

M^*	$a_1(1260)$		$\pi_2(1670)$		$\pi_2(2100)$	
	Pole mass (MeV)	$\Gamma_{\pi^+\pi^-\pi^0}$ (MeV)	Pole mass (MeV)	$\Gamma_{\pi^+\pi^-\pi^0}$ (MeV)	Pole mass (MeV)	$\Gamma_{\pi^+\pi^-\pi^0}$ (MeV)
Full	$1230 - 213i$	375.4	$1672 - 130i$	157.8	$2090 - 313i$	219.0
Isobar fit	$1230 - 100i$	371.9	$1672 - 97i$	151.2	$2090 - 261i$	217.0

isobar-fit model differ significantly from those of the unitary model from which the Dalitz plot data are generated. Their imaginary parts can differ by more than 100 MeV for $a_1(1260)$ and about 50 MeV for $\pi_2(1670)$ and $\pi_2(2100)$, indicating a large violation of the three-body unitarity. Note that the bare M^* mass [$M^0_{M^*}$ in Eq. (26)] does not enter the calculation of the Dalitz plots. Thus we choose $M^0_{M^*}$ for the isobar-fit model so that the real part of the pole is the same as that of the unitary model.

Some hadron models predict that the hybrid mesons can have quite different branching ratios from those of the ordinary mesons with radial excitations of the quark-antiquark pair [66]. Thus the parameters, $C_{\pi R,M^*}$, in Tables IV-VI can provide important information to distinguish the hybrid and/or exotic mesons from the ordinary mesons. The significant difference in the parameters between the unitary and isobar models indicates that we should use a unitary model to analyze the Dalitz plot distributions to search for the exotic mesons.

As discussed above, the importance of using an unitary model can be seen more clearly in comparing the $M^* \to \pi R$ amplitudes predicted by the two models. This is shown in Fig. 10. The $M^* \to \pi R$ amplitudes generated from unitary model must be complex because of multiple-scattering due to Z-diagram mechanisms, while those from isobar model can be chosen to be real (cf. footnote 4). Their differences in real parts can also be very different in some regions. The difference in the phase is more apparent. Even though non-zero phase could have been used in the isobar-fit model, as has been done in most isobar model analysis, the rather large dependence on the kinematics, which reflects the three-body unitarity, is beyond the capability of the isobar model to simulate. As we have noted, the phases of these amplitudes are crucial in using D meson decays to determine the phase γ of CKM matrix elements as a way to find physics beyond the Standard Model. The previously

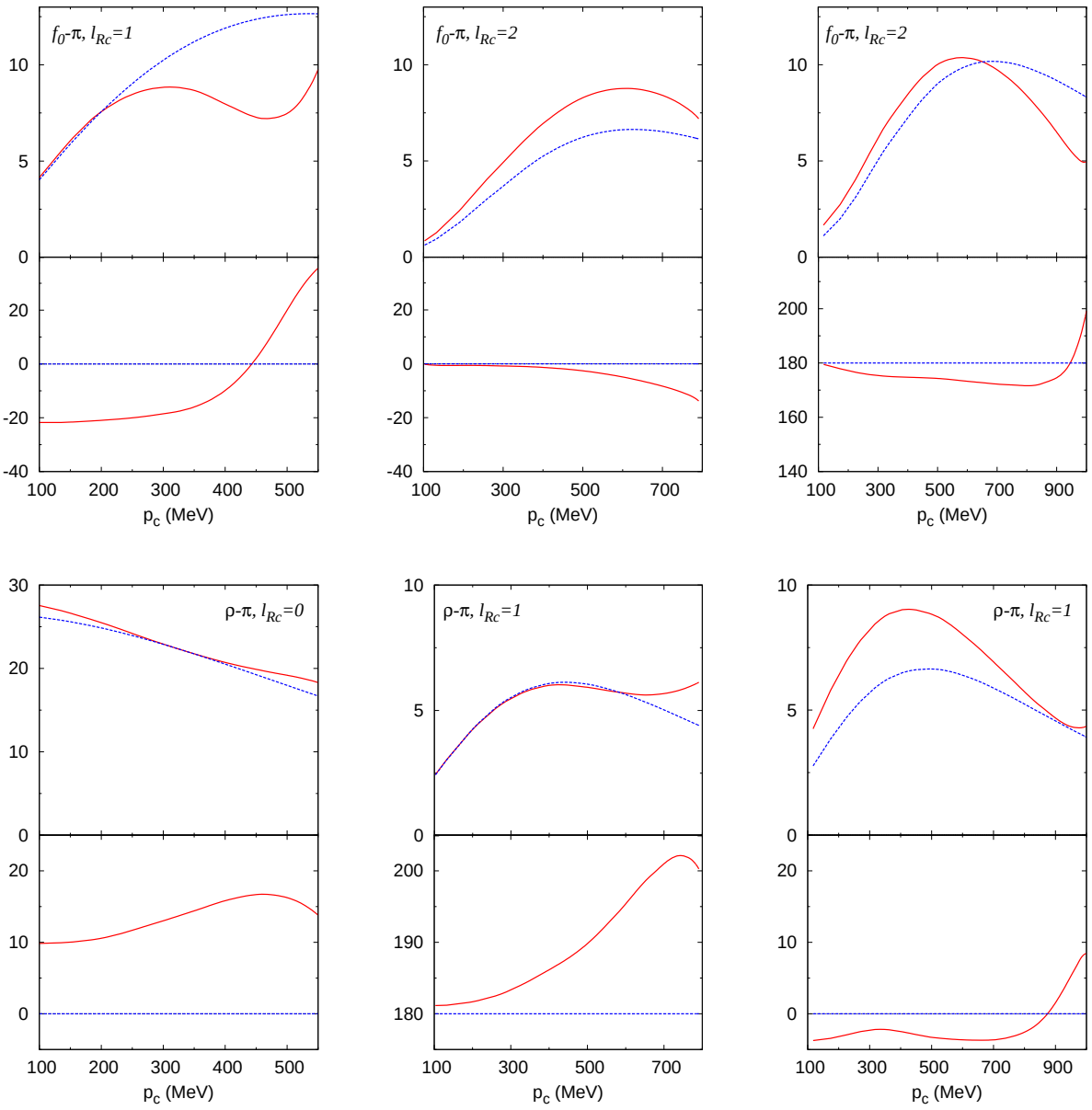

FIG. 10. (Color online) The partial wave $M^* \to cR$ vertices. The dressed [bare] vertices of the full [isobar-fit] model defined in Eq. (46) [Eq. (47)] are shown by the red solid [blue dashed] curves. The upper (lower) figure shows the absolute value (phase) of the vertices in arbitrary scale (degrees). The figures on the left, middle and right columns are for $a_1(1260)$, $\pi_2(1670)$ and $\pi_2(2100)$, respectively. The label in each figure specifies the cR state. We show the result for the bare $R = f_0$ or ρ of the lowest bare mass and $c = \pi$, and the relative orbital angular momentum of the cR is specified by l_{Rc}.

TABLE IX. Comparison between the total decay width of bare M^* ($\Gamma_{3\pi+\pi K\bar{K}}$) and twice of the imaginary part of the M^* self-energy ($-2\mathrm{Im}[\Sigma_{M^*}]$). Both of $\Gamma_{3\pi+\pi K\bar{K}}$ and Σ_{M^*} are calculated at $E = \mathrm{Re}[E_{M^*}]$, where E_{M^*} is a pole mass of a physical M^* listed in Table VIII. "Full" ("Isobar fit") is the results of the full unitary (isobar fit) model.

M^*	$a_1(1260)$		$\pi_2(1670)$		$\pi_2(2100)$	
	$\Gamma_{3\pi+\pi K\bar{K}}$ (MeV)	$-2\mathrm{Im}[\Sigma_{M^*}]$ (MeV)	$\Gamma_{3\pi+\pi K\bar{K}}$ (MeV)	$-2\mathrm{Im}[\Sigma_{M^*}]$ (MeV)	$\Gamma_{3\pi+\pi K\bar{K}}$ (MeV)	$-2\mathrm{Im}[\Sigma_{M^*}]$ (MeV)
Full	379.8	379.7	234.7	234.8	413.7	413.4
Isobar fit	378.4	266.2	227.4	198.7	434.5	379.1

extracted γ from $B^{\mp} \to D^0$ (or $\bar{D}^0$) $K^{\mp} \to (K^0_S\pi^+\pi^-)K^{\mp}$ has the uncertainty from the isobar model fitted to the D-decays. It is estimated to be 8.9° for Belle [23], 3° for BABAR [21]. Considering the difference in the phase, typically of $10^\circ \sim 20^\circ$ level, between the unitary and isobar models, it would be highly desirable to analyze the data with the unitary model.

Finally, let us examine the extent to which the three-body unitarity is satisfied by each model. We can examine this using Eqs. (31) and (32) which are satisfied by a unitary model. Within our current model developed for $a_1(1260)$, $\pi_2(1670)$ and $\pi_2(2100)$ decays, the total decay width ($\Gamma_{3\pi+\pi K\bar{K}}$) is the sum of $M^* \to 3\pi$ ($\Gamma_{3\pi}$) and $M^* \to \pi K\bar{K}$ ($\Gamma_{\pi K\bar{K}}$) widths. In the row labelled by "Full" of Table IX, we can see that the unitarity relation is satisfied within the numerical precision, as it should. On the other hand, for the isobar-fit model, the unitarity is rather badly violated as seen in the fifth row of Table IX, which raises a concern about the reliability of results obtained with the isobar model.

V. SUMMARY AND OUTLOOK

Starting with a model Hamiltonian with vertex interactions $f_{ab,R}$ and Γ_{cR,M^*} and two-body interactions $v_{c'R',cR}$, where R and M^* are the bare one-particle states and a, b, c are light pseudoscalar mesons (π, K, etc.), we have developed a unitary coupled-channels model for three-mesons decays of heavy mesons and excited meson states. By fitting the empirical amplitudes for meson-meson scattering such as $\pi\pi \to \pi\pi$, the vertex interactions $f_{ab,R}$, which

can generate resonances R in meson-meson scattering, are determined and used to predict the one-particle-exchange Z-diagram mechanisms $Z_{c'R',cR}(E)$. The scattering amplitudes $T_{c'R',cR}(E)$ are then calculated with $Z_{c'R',cR}(E)$ by solving a set of coupled-channels equations with the three-body unitarity condition satisfied exactly. The final state interactions of three-mesons from the decays of heavy mesons are then calculated from $T_{c'R',cR}(E)$. In the absence of the Z-diagram mechanisms, our decay amplitude is reduced to a form similar to that used in the isobar-model. This allows us to investigate the extent to which the commonly used isobar-model analysis is valid in extracting the properties of heavy mesons from the Dalitz plots of the measured three-mesons distributions. For strong decays of a heavy meson M^*, we present formula and procedures for investigating the importance of three-meson interactions in determining the resonance pole positions on complex energy Riemann surface.

The model has been applied to investigate three-pions decays of $a_1(1260)$, $\pi_2(1670)$ and $\pi_2(2100)$, and D^0 mesons. It was found that the Z-diagram mechanisms can change significantly the magnitudes and shapes of the Dalitz plots. For $D^0 \to \pi^+\pi^-\pi^0$, the changes in magnitudes can be a factor of about 1.6 in most of the phase space. For $a_1(1260)$, $\pi_2(1670)$ and $\pi_2(2100)$, the changes are about a factor of $1.3 \sim 1.6$ in magnitudes in the regions where meson-meson resonances $f_0(600)$, $\rho(770)$ and $f_2(1270)$ dominate. We have also examined differences between the unitary and isobar models for the case both of them produce the same Dalitz plot. We have demonstrated that decay amplitudes from the two models are significantly different, particularly in the phase. A proper estimate of the phase is particularly important for extracting the CKM phase γ from data of $B^\mp \to D^0$ (or $\bar{D}^0$) $K^\mp \to (K^0_S\pi^+\pi^-)K^\mp$ for which the D decay Dalitz plot is analyzed with a model. We have also shown that the three-body unitarity is rather largely violated in the isobar model. Finally, the resulting bare parameters which can be interpreted as characterizing the "intrinsic" quark-gluon substructure of heavy mesons are also very different between the unitary and isobar models.

Our results strongly indicate the need of re-analysis of the D meson decays using a unitary model to assess the results, such as the CKM matrix elements, obtained with the isobar model analysis [18–23]. It is also important re-analyze the 3-meson decays of all heavy mesons listed by PDG as a necessary step for establishing meson spectroscopy and exploring the hybrid or exotic mesons in the near future at JLab, GSI, and other possible

facilities. While the model presented in this work is more advanced than the models used in the previous analysis of three-meson decays processes, improvements are needed to make *quantitative* progress. We need to include the data associated with $K\bar{K}$ channels in determining our parameters. The approach for extending our formulation to include effects due to four-pions channels, which are considered to be important for determining scalar-isoscalar ($L = I = 0$) resonances, should be developed. For B-meson decays, an appropriate theoretical approach must be developed to describe $\pi\pi$ amplitudes at high energies where no data is available. Finally, our formulation is derived from applying a unitary transformation [67, 68] to a Hamiltonian defined within the relativistic quantum field theory. As discussed in Ref. [39], this method, as well as many well-studied three-dimensional reduction methods [69], is needed to derive *tractable* reaction models for solving complex reactions involving many channels and three-particle final states, with the unitarity maintained. Nevertheless, accuracy of these approximations should be investigated in the future.

ACKNOWLEDGMENTS

This work is supported by the U.S. Department of Energy, Office of Nuclear Physics Division, under Contract No. DE-AC02-06CH11357, and Contract No. DE-AC05-06OR23177 under which Jefferson Science Associates operates Jefferson Lab, and by the Japan Society for the Promotion of Science, Grant-in-Aid for Scientific Research(C) 20540270. HK acknowledges the support by the HPCI Stragetic Program (Field 5 "The Origin of Matter and the Universe") of Ministry of Education (Japan). This research used resources of the National Energy Research Scientific Computing Center, which is supported by the Office of Science of the U.S. Department of Energy under Contract No. DE-AC02-05CH11231, and resources provided on "Fusion," a 320-node computing cluster operated by the Laboratory Computing Resource Center at Argonne National Laboratory.

Appendix A: Relation between Σ_{M^*} and M^* decay amplitude

Here we derive Eq. (32). In the course of the derivation, we will see that Eq. (32) holds true only when the T-matrix (T') satisfies the unitarity relation. We start with the "decay"

width $\Gamma^{M^*}_{\rm tot}(E)$ of the *bare* M^* (not the physical resonance state) defined by

$$\Gamma^{M^*}_{\rm tot}(E) = 2\pi \sum_{abc} \delta(E - E_a - E_b - E_c) |T_{abc,M^*}(E)|^2. \tag{A1}$$

The amplitude T_{abc,M^*} is defined in Eq. (14), and it can be written as

$$T_{abc,M^*} = \langle abc|(1 + T'G_0)H'|M^*\rangle \ , \tag{A2}$$

where G_0 is the free Green function, and the reaction T-matrix (T') has been defined in Eq. (5). By using Eqs. (A1) and (A2) together with the unitarity relation

$$T' - T'^\dagger = -2\pi i T' \delta(E - H_0) T'^\dagger, \tag{A3}$$

and the equality

$$G_0 - G_0^\dagger = -2\pi i \delta(E - H_0), \tag{A4}$$

we arrive at Eq. (32) as

$$\begin{aligned}
\Gamma^{M^*}_{\rm tot}(E) &= 2\pi \sum_{abc} \delta(E - E_a - E_b - E_c) \left|T_{abc,M^*}(E)\right|^2 \\
&= 2\pi \sum_{abc} \delta(E - E_a - E_b - E_c) \left|\langle M^*|H'(1 + G_0^\dagger T'^\dagger)|abc\rangle\right|^2 \\
&= 2\pi \langle M^*|H'(1 + G_0^\dagger T'^\dagger)\delta(E - H_0)(1 + T'G_0)H'|M^*\rangle \\
&= i\left[\langle M^*|H'G_0(1 + T'G_0)H'|M^*\rangle - \langle M^*|H'(1 + G_0^\dagger T'^\dagger)G_0^\dagger H'|M^*\rangle\right] \\
&= -2\ {\rm Im}\left[\langle M^*|H'G_0(1 + T'G_0)H'|M^*\rangle\right] \\
&= -2\ {\rm Im}\left[\Sigma_{M^*}(E)\right].
\end{aligned} \tag{A5}$$

In the last step we have used the definition of $\Sigma_{M^*}(E)$ given in Eq. (27).

Appendix B: Dalitz plot

Here we summarize the formulae for calculating Dalitz plots. The differential decay width of a heavy meson M^* (E: mass; S_{M^*}: spin) at rest decaying to three (pseudo) scalar mesons, $M^*(\vec{0}, E) \to a(\vec{p}_a) + b(\vec{p}_b) + c(\vec{p}_c)$, where we consider only (pseudo) scalar mesons for the final state, can be expressed as

$$\begin{aligned}
d\Gamma_{M^*} = \frac{1}{2E} \frac{d^3p_a}{(2\pi)^3 2E_a(p_a)} \frac{d^3p_b}{(2\pi)^3 2E_b(p_b)} \frac{d^3p_c}{(2\pi)^3 2E_c(p_c)} \frac{\mathcal{B}}{2S_{M^*}+1} \sum_{S^z_{M^*}} |\mathcal{M}_{abc,M^*}|^2 \\
\times (2\pi)^4 \delta(E - E_a(p_a) - E_b(p_b) - E_c(p_c)) \delta^3(\vec{0} - \vec{p}_a - \vec{p}_b - \vec{p}_c),
\end{aligned} \tag{B1}$$

where $\mathcal{M}_{abc,M^*}$ is the invariant amplitude of the decay; $\mathcal{B}$ is the Bose factor for the final mesons. For example, when the three final mesons are identical, $\mathcal{B} = 1/3!$. With a variable transformation, we obtain the double differential decay width distribution (Dalitz plot density) for the unpolarized decay given by

$$\frac{d^2\Gamma_{M^*}}{dm_{ab}^2 dm_{bc}^2} = \frac{1}{(2\pi)^3}\frac{1}{32E^3}\frac{\mathcal{B}}{2S_{M^*}+1}\sum_{S^z_{M^*}}|\mathcal{M}_{abc,M^*}|^2, \tag{B2}$$

where m_{ab} (m_{bc}) is the invariant mass of the ab (bc) pair. The invariant amplitude is related to the decay amplitude defined in Eq. (23) or Eq. (43) by

$$\mathcal{M}_{abc,M^*} = -(2\pi)^3\sqrt{2E}\sqrt{2E_a(p_a)}\sqrt{2E_b(p_b)}\sqrt{2E_c(p_c)}T_{abc,M^*}. \tag{B3}$$

The meson labels a, b, c specify the momentum (p_x), the mass (m_x), and the isospin (t_x) of the meson $x = a, b, c$.

Next, we summarize relations between kinematic variables. For a given value of m_{ab}^2, the range of m_{bc}^2 is determined by its values when $\vec{p}_b$ is parallel or anti-parallel to $\vec{p}_c$:

$$\begin{aligned}(m_{bc}^2)_{\max} &= (E_b^* + E_c^*)^2 - \left(\sqrt{E_b^{*2} - m_b^2} - \sqrt{E_c^{*2} - m_c^2}\right)^2,\\ (m_{bc}^2)_{\min} &= (E_b^* + E_c^*)^2 - \left(\sqrt{E_b^{*2} - m_b^2} + \sqrt{E_c^{*2} - m_c^2}\right)^2,\end{aligned} \tag{B4}$$

with

$$\begin{aligned}E_b^* &= \frac{1}{2m_{ab}}(m_{ab}^2 - m_a^2 + m_b^2),\\ E_c^* &= \frac{1}{2m_{ab}}(E^2 - m_{ab}^2 + m_c^2),\end{aligned} \tag{B5}$$

being the energies of the particles b and c in the center-of-mass frame of the ab pair, respectively. For a given set of m_{ab} and m_{bc}, the momenta of the final particles are

$$\begin{aligned}p_a &= \frac{1}{2E}\sqrt{[E^2 - (m_{bc} + m_a)^2][E^2 - (m_{bc} - m_a)^2]},\\ p_c &= \frac{1}{2E}\sqrt{[E^2 - (m_{ab} + m_c)^2][E^2 - (m_{ab} - m_c)^2]},\\ p_b &= \sqrt{E_b^2 - m_b^2} = \sqrt{(E - E_a - E_c)^2 - m_b^2},\\ \cos\theta_{ab} &= \frac{1}{2p_a p_b}\left[(E - E_a - E_b)^2 - m_c^2 - p_a^2 - p_b^2\right],\end{aligned} \tag{B6}$$

where θ_{ab} is the angle between $\vec{p}_a$ and $\vec{p}_b$. Taking $\vec{p}_a$ on the xz-plane, we have

$$\vec{p}_a = p_a(\sin\theta_a, 0, \cos\theta_a),$$

$$\vec{p}_b = p_b(\cos\theta_a \sin\theta_{ab}\cos\phi_{ab} + \sin\theta_a \cos\theta_{ab}, \sin\theta_{ab}\sin\phi_{ab},$$
$$-\sin\theta_a \sin\theta_{ab}\cos\phi_{ab} + \cos\theta_a\cos\theta_{ab}),$$
$$\vec{p}_c = -\vec{p}_a - \vec{p}_b, \tag{B7}$$

where ϕ_{ab} is the azimuthal angle of $\vec{p}_{b'}$ which is obtained by rotating $\vec{p}_b$ around y-axis by $-\theta_a$. To calculate the differential decay width for the unpolarized decay [Eq. (B2)], one may set $\theta_a = 0$ and $\phi_{ab} = 0$.

Appendix C: *Z*-diagrams

1. Definition

The matrix element of the Z-diagram for a transition process, $R(-\vec{p}_c)+c(\vec{p}_c) \to R'(-\vec{p}_{c'})+ c'(\vec{p}_{c'})$, is given by

$$\langle R'(-\vec{p}_{c'}, s^z_{R'}, t^z_{R'}); c'(\vec{p}_{c'}, 0, t^z_{c'})|Z^{c''}(E)|R(-\vec{p}_c, s^z_R, t^z_R); c(\vec{p}_c, 0, t^z_c)\rangle =$$
$$\langle R'(-\vec{p}_{c'}, s^z_{R'}, t^z_{R'})|f_{R',c''c}|c(\vec{p}_c, 0, t^z_c); c''(\vec{p}_{c''}, 0, t^z_{c''})\rangle$$
$$\times \frac{1}{E - E_c(p_c) - E_{c'}(p_{c'}) - E_{c''}(p_{c''}) + i\epsilon}$$
$$\times \langle c'\left(\vec{p}_{c'}, 0, t^z_{c'}\right); c''\left(\vec{p}_{c''}, 0, t^z_{c''}\right)|f_{c'c'',R}|R\left(-\vec{p}_c, s^z_R, t^z_R\right)\rangle. \tag{C1}$$

Here c'' is the exchanged meson; s^z_R (t^z_R) is the z-component of the spin (isospin) of the particle R; t^z_c is the z-component of the isospin of the particle c; $\vec{p}_{c''} = -\vec{p}_c - \vec{p}_{c'}$. The vertices are expressed by

$$\langle c'(\vec{p}_{c'}, 0, t^z_{c'}); c''(\vec{p}_{c''}, 0, t^z_{c''})|f_{c'c'',R}|R\left(-\vec{p}_c, s^z_R, t^z_R\right)\rangle =$$
$$J_R(p_{c'}, p_{c''}, q_c)\langle t_{c'}t^z_{c'}t_{c''}t^z_{c''}|t_R t^z_R\rangle Y_{s_R s^z_R}(\hat{q}_c)\tilde{f}_{c'c'',R}(q_c), \tag{C2}$$
$$\langle R'\left(-\vec{p}_{c'}, s^z_{R'}, t^z_{R'}\right)|f_{R',c''c}|c\left(\vec{p}_c, 0, t^z_c\right); c''\left(\vec{p}_{c''}, 0, t^z_{c''}\right)\rangle =$$
$$J_{R'}(p_c, p_{c''}, q_{c'})\langle t_{c''}t^z_{c''}, t_c t^z_c|t_{R'}t^z_{R'}\rangle Y^*_{s_{R'}s^z_{R'}}(\hat{q}_{c'})\tilde{f}_{R',c''c}(q_{c'}). \tag{C3}$$

The above equations are the same as Eq. (44), and $\tilde{f}$ is related to the $\pi\pi$ model [Eq. (35)] through Eq. (39). Here $\vec{q}_c$ is the meson momentum in the center of mass of the two-meson ($c'c''$) sub-system from the $R(-\vec{p}_c) \to c'(\vec{p}_{c'}) + c''(\vec{p}_{c''})$ decay. The factor J_R appears as a result of the Lorentz transformation of the vertex, and is given by

$$J_R(p_x, p_{c''}, q_y) = \sqrt{\frac{E_x(q_y)E_{c''}(q_y)m_R}{E_x(p_x)E_{c''}(p_{c''})E_R(p_y)}}, \tag{C4}$$

with $x, y = c$ or c'. Using the Lorentz transformation, we have

$$\vec{q}_c = \vec{p}_{c'} - \rho(-\vec{p}_c, \vec{p}_{c'})\vec{p}_c \equiv \kappa_c \vec{p}_c + \lambda_c \vec{p}_{c'}, \tag{C5}$$

$$-\vec{q}_{c'} = \vec{p}_c - \rho(-\vec{p}_{c'}, \vec{p}_c)\vec{p}_{c'} \equiv \kappa_{c'} \vec{p}_c + \lambda_{c'} \vec{p}_{c'}. \tag{C6}$$

where

$$\rho(\vec{P}, \vec{p}_x) = \frac{1}{\xi(\vec{P}, \vec{p}_x)} \left[\frac{\vec{P} \cdot \vec{p}_x}{\xi(\vec{P}, \vec{p}_x) + E_x(p_x) + E_{c''}(|\vec{P} - \vec{p}_x|)} - E_x(p_x) \right], \tag{C7}$$

and

$$\xi(\vec{P}, \vec{p}_x) = \sqrt{\left[E_x(p_x) + E_{c''}(|\vec{P} - \vec{p}_x|) \right]^2 - \vec{P}^2}. \tag{C8}$$

The signs attached to $\vec{p}_c$ and $\vec{p}_{c'}$ in Eqs. (C5) and (C6), and the ordering of isospins in the Clebsch-Gordan coefficients in Eqs. (C2) and (C3) matters for the phases of the $\rho \leftrightarrow \pi\pi$ interaction, and are taken consistently with the $\rho\pi\pi$ interaction Lagrangian. To take phases appropriately is important for giving the correct phases to the amplitudes.

2. Partial wave decomposition of Z potential

We define the partial-wave expansion of Eq. (C1) as

$$\begin{aligned}
\langle R'(-\vec{p}_{c'}, s^z_{R'}, t^z_{R'}); c'(\vec{p}_{c'}, 0, t^z_{c'}) | Z^{c''}(E) | R(-\vec{p}_c, s^z_R, t^z_R); c, (\vec{p}_c, 0, t^z_c) \rangle = \\
\sum_{TT^z} \sum_{JJ^z} \sum_{l'l'^z ll^z} \langle t_R t^z_R t_c t^z_c | TT^z \rangle \langle t_{R'} t^z_{R'} t_{c'} t^z_{c'} | TT^z \rangle \\
\times \langle l l^z s_R s^z_R | J J^z \rangle \langle l' l'^z s_{R'} s^z_{R'} | J J^z \rangle \\
\times Y_{l',l'^z}(\hat{p}_{c'}) Y^*_{l,l^z}(\hat{p}_c) Z^{c'',JPT}_{(c'R')_{l'},(cR)_l}(p_{c'}, p_c).
\end{aligned} \tag{C9}$$

Performing some manipulations, we obtain

$$\begin{aligned}
Z^{c'',JPT}_{(c'R')_{l'},(cR)_l}(p_{c'}, p_c) = (-1)^{t_{c''} - t_R + t_{c'}} \sqrt{(2t_R + 1)(2t_{R'} + 1)} W(t_c t_{R'} t_R t_{c'}; t_{c''} T) \\
\times (-1)^{s_{R'}} \sqrt{(2s_{R'} + 1)(2s_R + 1)(2l' + 1)(2l + 1)} \\
\times \sum_{l_a, l_b, L', L'', j} (2j + 1)(2L' + 1)(2L'' + 1) \sqrt{\frac{(2s_{R'} + 1)!(2s_R + 1)!}{(2l_a)!(2s_{R'} - 2l_a)!(2l_b)!(2s_R - 2l_b)!}} \\
\times \begin{pmatrix} l' & l_a & L' \\ 0 & 0 & 0 \end{pmatrix} \begin{pmatrix} l & l_b & L'' \\ 0 & 0 & 0 \end{pmatrix} \begin{pmatrix} s_R - l_b & j & L' \\ 0 & 0 & 0 \end{pmatrix} \begin{pmatrix} s_{R'} - l_a & j & L'' \\ 0 & 0 & 0 \end{pmatrix} \\
\times \begin{Bmatrix} l' & l_a & L' \\ s_{R'} - l_a & J & s_{R'} \end{Bmatrix} \begin{Bmatrix} l & l_b & L'' \\ s_R - l_b & J & s_R \end{Bmatrix} \begin{Bmatrix} L'' & s_R - l_b & J \\ L' & s_{R'} - l_a & j \end{Bmatrix} F^{l_a, l_b}_j,
\end{aligned} \tag{C10}$$

where we have used $(-1)^{l+l'+s_R+s_{R'}} = 1$ from the parity conservation. We have introduced $F_j^{l_a,l_b}$ and B defined by

$$F_j^{l_a,l_b} = \frac{1}{2}\int_{-1}^{1} dx \frac{BP_j(x)}{E - E_c(p_c) - E_{c'}(p_{c'}) - E_{c''}(p_{c''}) + i\epsilon}, \tag{C11}$$

$$\begin{aligned} B = {} & J(p_c, p_{c''}, q_{c'}) \tilde{f}^{s_{R'} t_{R'}}_{cc'',R'}(q_{c'}) J(p_{c'}, p_{c''}, q_c) \tilde{f}^{s_R t_R}_{R,c'c''}(q_c) \\ & \times (\lambda_{c'} p_{c'})^{l_a} (\kappa_{c'} p_{c'})^{s_{R'} - l_a} (\lambda_c p_{c'})^{s_R - l_b} (\kappa_c p_c)^{l_b} (q_c)^{-s_R} (q_{c'})^{-s_{R'}}, \end{aligned} \tag{C12}$$

where $P_j(x)$ is the Legendre function of the degree j.

---

[1] E. Klempt and A. Zaitsev, Phys. Rept. **454**, 1 (2007).

[2] S. U. Chung *et al.* (E852 Collaboration), Phys. Rev. Lett. **81**, 5760 (1998).

[3] S. U. Chung *et al.* (E852 Collaboration), Phys. Rev. D **65**, 072001 (2002).

[4] A. R. Dzierba *et al.*, Phys. Rev. D **73**, 072001 (2006).

[5] D. S. Carman (The Gluex Collaboration), AIP Conf. Proc. **814**, 173 (2006).

[6] M. Nozar *et al.* (CLAS Collaboration), Phys. Rev. Lett. **102**, 102002 (2009).

[7] W. Dunnweber and F. Meyer-Wildhagen, AIP Conf. Proc. **717**, 388 (2004).

[8] K. L. Au, D. Morgan, and M. R. Pennington, Phys. Rev. D **35**, 1633 (1987).

[9] P. Guo, R. Mitchell, and A. P. Szczepaniak, Phys. Rev. D **82**, 094002 (2010).

[10] M. Alekseev *et al.* (COMPASS Collaboration), Phys. Rev. Lett. **104**, 241803 (2010).

[11] J. Z. Bai *et al.* (BES Collaboration), Phys. Rev. D **70**, 012005 (2004).

[12] B. Aubert *et al.* (BABAR Collaboration), Phys. Rev. D **70**, 072004 (2004).

[13] P. Frabetti *et al.* (E687 Collaboration), Phys. Lett. **B331**, 217 (1994).

[14] J. C. Anjos *et al.* (E691 Collaboration), Phys. Rev. D **48**, 56 (1993).

[15] J. Adler *et al.* (Mark III Collaboration), Phys. Lett. **B196**, 107 (1987).

[16] D. J. Summers *et al.*, Phys. Rev. Lett. **52**, 410 (1984).

[17] S. Kopp *et al.* (CLEO Collaboration), Phys. Rev. D **63**, 092001 (2001).

[18] B. Aubert *et al.* (BABAR Collaboration), Phys. Rev. Lett. **95**, 121802 (2005).

[19] B. Aubert *et al.* (BABAR Collaboration), Phys. Rev. Lett. **99**, 251801 (2007).

[20] B. Aubert *et al.* (BABAR Collaboration), Phys. Rev. D **78**, 034023 (2008).

[21] P. del Amo Sanchez *et al.* (BABAR Collaboration), Phys. Rev. Lett. **105**, 121801 (2010).

[22] A. Poluektov *et al.* (Belle Collaboration), Phys. Rev. D **73**, 112009 (2006).

[23] A. Poluektov *et al.* (Belle Collaboration), Phys. Rev. D **81**, 112002 (2010).

[24] A. Garmash *et al.* (Belle Collaboration), Phys. Rev. D **65**, 092005 (2002).

[25] A. Garmash *et al.* (Belle Collaboration), Phys. Rev. D **69**, 012001 (2004).

[26] A. Garmash *et al.* (Belle Collaboration), Phys. Rev. Lett. **96**, 251803 (2006).

[27] A. Garmash *et al.* (Belle Collaboration), Phys. Rev. D **71**, 092003 (2005).

[28] K. Abe *et al.* (Belle Collaboration), (2005), arXiv:hep-ex/0509047.

[29] A. Garmash *et al.* (Belle Collaboration), Phys. Rev. D **75**, 012006 (2007).

[30] E. Eckhart *et al.* (CLEO Collaboration), Phys. Rev. Lett. **89**, 251801 (2002).

[31] B. Aubert *et al.* (BABAR Collaboration), Phys. Rev. Lett. **91**, 051801 (2003).

[32] B. Aubert *et al.* (BABAR Collaboration), Phys. Rev. D **72**, 072003 (2005); **74**, 099903(E) (2006).

[33] B. Aubert *et al.* (BABAR Collaboration), Phys. Rev. D **73**, 031101 (R) (2006).

[34] B. Aubert *et al.* (BABAR Collaboration), Phys. Rev. D **78**, 012004 (2008).

[35] B. Aubert *et al.* (BABAR Collaboration), Phys. Rev. D **78**, 052005 (2008).

[36] B. El-Bennich *et al.*, Phys. Rev. D **79**, 094005 (2009).

[37] A. W. Thomas, ed., *Modern Three-Hadron Physics* (Springer, 1977).

[38] H. Garcilazo and T. Mizutani, πNN *Systems* (World Scientific, 1990).

[39] A. Matsuyama, T. Sato, and T.-S. H. Lee, Phys. Rept. **439**, 193 (2007).

[40] B. Juliá-Díaz, T.-S. H. Lee, A. Matsuyama, and T. Sato, Phys. Rev. C **76**, 065201 (2007).

[41] M. Doring, C. Hanhart, F. Huang, S. Krewald, and U. G. Meissner, Nucl. Phys. **A829**, 170 (2009).

[42] T. Frederico, K. Guimarães, W. de Paula, I. Bediaga, A. dos Reis, P. Magalhães, M. Robilotta, A. Delfino, and L. Tomio, PoS **LC2010**, 005 (2010).

[43] P. Magalhães, M. R. Robilotta, K. S. F. F. Guimarães, T. Frederico, W. de Paula, I. Bediaga, A. C. dos Reis, C. M. Maekawa, and G. R. S. Zarnauskas, (2011), arXiv:1105.5120 [hep-ph].

[44] H. Feshbach, Ann. Phys. (N.Y.) **5**, 357 (1958).

[45] H. Feshbach, Ann. Phys. (N.Y.) **19**, 287 (1962).

[46] M. Kobayashi, T. Sato, and H. Ohtsubo, Prog. Theor. Phys. **98**, 927 (1997).

[47] N. Suzuki, T. Sato, and T. S. H. Lee, Phys. Rev. C **79**, 025205 (2009).

[48] N. Suzuki, T. Sato, and T. S. H. Lee, Phys. Rev. C **82**, 045206 (2010).

[49] J. Gasser and H. Leutwyler, Nucl. Phys. **B250**, 465 (1985).

[50] M. Bando, T. Kugo, and K. Yamawaki, Phys. Pep. **164**, 217 (1988).

[51] G. Ecker, J. Gasser, A. Pich, and E. De Rafael, Nucl. Phys. **B321**, 311 (1989).

[52] V. Bernard, N. Kaiser, and U.-G. Meißner, Nucl. Phys. **B364**, 283 (1991).

[53] G. Grayer *et al.*, Nucl. Phys. B **75**, 189 (1974).

[54] B. Hyams *et al.* , Nucl. Phys. B **64**, 134 (1973).

[55] J.R. Batley *et al.* (The NA48/2 Collaboration), Eur. Phys. J. C **54**, 411 (2008).

[56] H. Becker *et al.*, Nucl. Phys. B **151**, 46 (1979).

[57] A. Badalyan, L. Kok, M. Polikarpov, and Y. Simonov, Phys. Rept. **82**, 31 (1982).

[58] K. Nakamura *et al.* (Particle Data Group), J. Phys. **G37**, 075021 (2010).

[59] J. A. Oller, E. Oset, and J. R. Peláez, Phys. Rev. D **59**, 074001 (1999); **74**, 099903(E) (1999).

[60] R. Kamiński, L. Leśniak, and J. P. Maillet, Phys. Rev. D **50**, 3145 (1994).

[61] J. Weinstein and N. Isgur, Phys. Rev. Lett. **48**, 659 (1982).

[62] C. Zemach, Phys. Rev. **133**, B1201 (1964).

[63] A. Giri, Y. Grossman, A. Soffer, and J. Zupan, Phys. Rev. D **68**, 054018 (2003).

[64] A. Bondar and A. Poluektov, Eur. Phys. J. C **47**, 347 (2006).

[65] A. Bondar and A. Poluektov, Eur. Phys. J. C **55**, 51 (2008).

[66] T. Barnes, F. E. Close, P. R. Page, and E. S. Swanson, Phys. Rev. D **55**, 4157 (1997).

[67] M. Kobayashi, T. Sato, and H. Ohtsubo, Prog. Theor. Phys. **98**, 927 (1997).

[68] T. Sato and T.-S. H. Lee, Phys. Rev. C **54**, 2660 (1996).

[69] A. Klein and T.-S. H. Lee, Phys. Rev. D **10**, 4308 (1974).